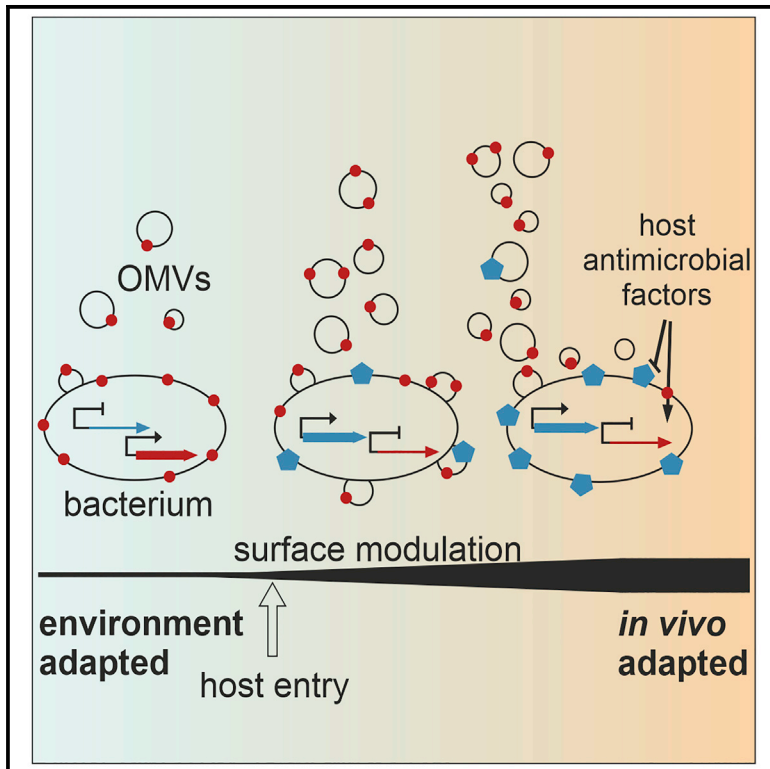


Cell Host & Microbe

Outer Membrane Vesiculation Facilitates Surface Exchange and *In Vivo* Adaptation of *Vibrio cholerae*

Graphical Abstract



Authors

Franz G. Zingl, Paul Kohl,
Fatih Cakar, ..., Ziqiang Guan,
Joachim Reidl, Stefan Schild

Correspondence

stefan.schild@uni-graz.at

In Brief

Upon infection, *Vibrio cholerae* must alter its surface profile to evade host defenses and adapt to the gastrointestinal environment. Zingl et al. show that increased release of outer membrane vesicles upon host entry allows the bacteria to rapidly modify their cell surface, thus increasing *in vivo* adaptation and colonization fitness.

Highlights

- Phospholipid transport of *Vibrio cholerae* is silenced upon host entry
- Reduced transporter activity triggers OMV release and increases colonization fitness
- Increased vesiculation accelerates modulation of cell surface composition
- Hypervesiculation leads to faster adaptation to host defense mediators

Outer Membrane Vesiculation Facilitates Surface Exchange and *In Vivo* Adaptation of *Vibrio cholerae*

Franz G. Zingl,¹ Paul Kohl,¹ Fatih Cakar,¹ Deborah R. Leitner,¹ Fabian Mitterer,¹ Katherine E. Bonnington,² Gerald N. Rechberger,^{1,3} Meta J. Kuehn,² Ziqiang Guan,⁴ Joachim Reidl,^{1,5} and Stefan Schild^{1,5,6,*}

¹Institute of Molecular Biosciences, University of Graz, 8010 Graz, Austria

²Duke University Medical Center, Durham, NC 27710, USA

³Center for Explorative Lipidomics, BioTechMed Graz, 8010 Graz, Austria

⁴Department of Biochemistry, Duke University Medical Center, Durham, NC 27710, USA

⁵BioTechMed Graz, 8010 Graz, Austria

⁶Lead Contact

*Correspondence: stefan.schild@uni-graz.at

<https://doi.org/10.1016/j.chom.2019.12.002>

SUMMARY

Gram-negative bacteria release outer membrane vesicles into the external milieu to deliver effector molecules that alter the host and facilitate virulence. Vesicle formation is driven by phospholipid accumulation in the outer membrane and regulated by the phospholipid transporter VacJ/Yrb. We use the facultative human pathogen *Vibrio cholerae* to show that VacJ/Yrb is silenced early during mammalian infection, which stimulates vesiculation that expedites bacterial surface exchange and adaptation to the host environment. Hypervesiculating strains rapidly alter their bacterial membrane composition and exhibit enhanced intestinal colonization fitness. This adaptation is exemplified by faster accumulation of glycine-modified lipopolysaccharide (LPS) and depletion of outer membrane porin OmpT, which confers resistance to host-derived antimicrobial peptides and bile, respectively. The competitive advantage of hypervesiculation is lost upon pre-adaptation to bile and antimicrobial peptides, indicating the importance of these adaptive processes. Thus, bacteria use outer membrane vesiculation to exchange cell surface components, thereby increasing survival during mammalian infection.

INTRODUCTION

It is widely accepted that all domains of life produce membrane vesicles. Extracellular vesicles released from the outer membrane (OM) of gram-negative bacteria, generally referred to as outer membrane vesicles (OMVs), are one of the best-studied vesicles (Toyofuku et al., 2019). These spherical, non-living facsimiles of the bacterial donor cell have been mainly characterized as delivery vehicles for effector molecules, such as quorum-sensing signals, nucleic acids, degradative enzymes, inflammatory agents, or toxins (Jan, 2017; Schwechheimer and Kuehn, 2015). Consequently, OMVs have been attributed a role in intra- and inter-spe-

cies communication, horizontal gene transfer, nutrient acquisition, immunomodulation, and virulence (Kulp and Kuehn, 2010).

Recently, our group identified a conserved mechanism for OMV release based on phospholipid accumulation in the OM because of inactivation or transcriptional silencing of the VacJ/Yrb ATP-binding cassette (ABC) transporter, also known as the maintenance of OM lipid asymmetry (Mla) system (Figure 1A) (Roier et al., 2016). This highly conserved trafficking system of Gram-negative bacteria was originally reported to shuttle phospholipids from the outer to the inner membrane to maintain the lipid asymmetry of the OM (Malinverni and Silhavy, 2009). In contrast to this view, recent data suggest that the VacJ/Yrb transport system can also export phospholipids from the inner membrane (Hughes et al., 2019; Kamischke et al., 2019). Although mechanistic details remain to be elucidated, it is evident that inactivation or downregulation of the VacJ/Yrb transporter results in elevated OMV levels (Roier et al., 2016). Importantly, iron depletion in several Gram-negative bacteria (i.e., *Escherichia coli*, *Vibrio cholerae*, and *Haemophilus influenzae*) triggers a ferric uptake regulator (Fur)-dependent repression of the VacJ/Yrb transporter, leading to increased OMV release (Roier et al., 2016). Iron limitation is a common stressor for bacterial pathogens during host colonization; therefore, we predicted that transcriptional silencing of the *vacJ* and *yrbF-B* genes and the resulting boost in vesiculation should occur upon host entry. In support of this model, *H. influenzae* was shown to lower expression levels of the VacJ/Yrb transporter during nasopharyngeal colonization (Roier et al., 2016).

Benefits driving bacteria to alter vesiculation *in vivo* remain to be elucidated. In the case of *H. influenzae*, higher OMV levels correlated with increased serum resistance (Roier et al., 2016). Thus, increased vesiculation might facilitate bacterial proliferation in the nasopharynx.

Given that bacteria discharge components of the periplasm and OM into the extracellular milieu via OMVs, increased vesiculation could also represent a previously overlooked adaptation to modulate their cell surface composition. This strategy could be quite valuable as bacteria are frequently challenged to adapt to diverse conditions with different requirements along their life cycle (Conner et al., 2016; O'Connor and McClean, 2017). The need to change surface components upon host entry, e.g., capsule, flagella, fimbriae, pili, lipopolysaccharide (LPS)

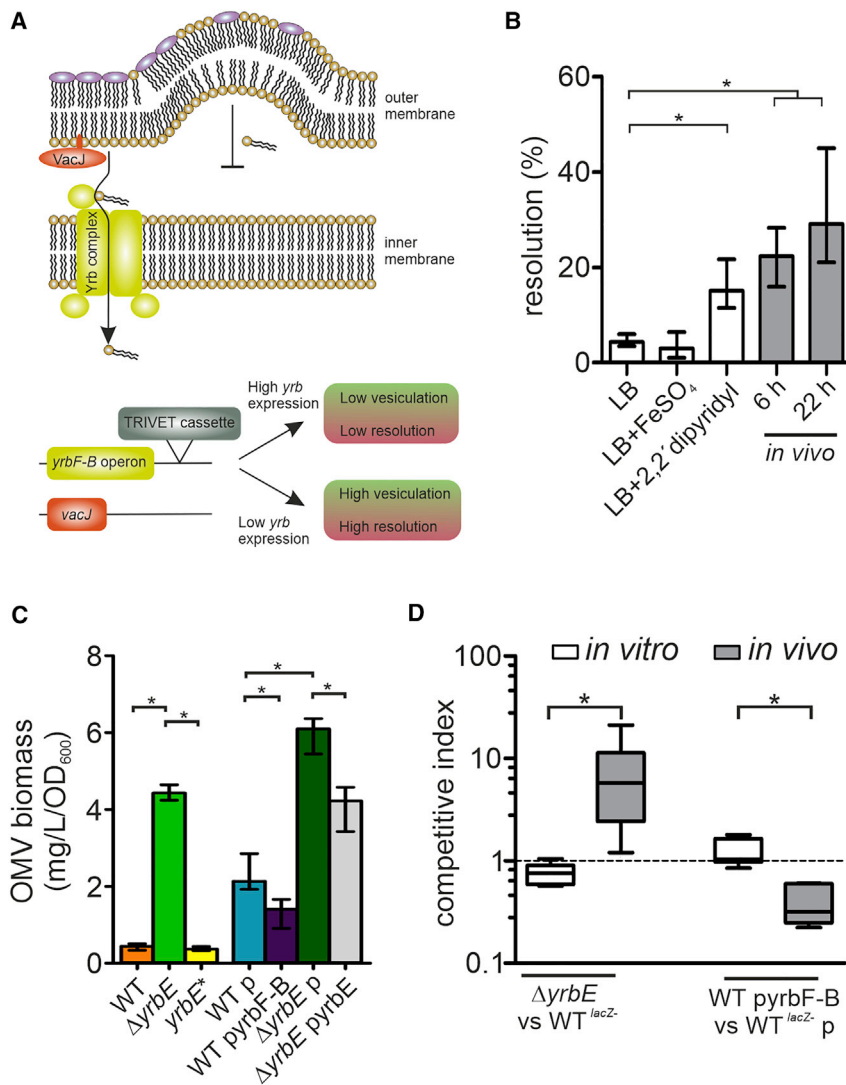


Figure 1. Silencing of *yrbF-B* Occurs upon Host Entry, and Colonization Fitness Varies Inversely with Transporter Activity

(A) Schematic overview of the phospholipid transporter encoded by the *vacJ* and *yrbFEDCB* (*yrbF-B* operon) genes. The *VacJ/Yrb* transporter (also known as the *Mla* system) shuttles phospholipids from the outer membrane (OM) back to the inner membrane. High expression is associated with low vesiculation, whereas low expression or inactivation of the transporter results in phospholipid accumulation in the OM outer leaflet promoting vesiculation. Insertion of the TRIVET reporter cassette downstream of the *yrb* locus allows monitoring of its transcriptional activity using excision of an antibiotic resistance cassette (resolution) as a readout.

(B) Transcriptional regulation of the *yrbF-B* operon was analyzed by the recombination-based *in vivo* reporter system TRIVET, which results in increased reporter resolution upon transcriptional repression of the *yrbF-B* operon (Cakar et al., 2018). Shown are resolution frequencies of strain *Vc_res1_TRIVET yrbF::tpc* grown for 22 h in regular LB and LB with high-(FeSO₄) or low-(2,2'-dipyridyl) iron concentrations as well as *in vivo* 6 and 22 h post-infection. Shown is the median ± interquartile range (IQR) (n = 6; *p < 0.05). See also Figure S1.

(C) OMV quantification (Bradford) for WT, $\Delta yrbE$, *yrbE*⁺, WT with empty vector (P), WT with *yrbF-B* overexpression plasmid (*pyrB-B*), $\Delta yrbE$ with empty vector (P), and $\Delta yrbE$ with expression plasmid (*pyrB-E*) after 8-h cultivation. Shown is the median ± IQR (*p < 0.05) with the following number of biological replicates: n = 9 for WT and WT p; n = 6 for $\Delta yrbE$, *yrbE*⁺, $\Delta yrbE$ p, and $\Delta yrbE$ *pyrB-E*; and n = 8 for WT *pyrB-B*.

(D) Competition indices of *in vitro* (LB) and *in vivo* (murine model) assays are shown as a boxplot with whiskers (*p < 0.05) with the following number of biological replicates: n = 8 for all *in vitro* competitions, n = 10 for the *in vivo* competitions of WT^{lacZ-} and $\Delta yrbE$, and n = 6 for the *in vivo* competitions of WT^{lacZ-} p and WT *pyrB-B*. Strains used for the competition are indicated on the x axis.

modifications, metabolite uptake systems, and porins, is especially apparent for facultative bacterial pathogens (King and Roberts, 2016; Phillips et al., 2019).

Along its life cycle, the facultative human pathogen *V. cholerae* transits between the aquatic reservoir and the human intestinal tract. To assess the impact of vesiculation on surface modulation specifically upon host entry, we used *V. cholerae* as a model organism and focused on the initial stage of infection. Once ingested, *V. cholerae* modulates its surface profile to adapt to antimicrobial factors present in the gut. For example, the expression of two abundant OM porins *OmpU* and *OmpT* are inversely regulated upon host entry. This *OmpU/T* switch is directly controlled by the virulence regulator *ToxR* and is decisive for the bacterium to achieve bile resistance *in vivo* (Provenzano and Klose, 2000). Unlike *OmpT*, *OmpU* is an anion-selective porin that restricts the passage of negatively charged compounds (Simonet et al., 2003). Thus, depletion of *OmpT* in the OM makes *V. cholerae* less vulnerable to bile salts. Concomitantly, upon host entry, *V. cholerae* activates transcription of

ompU and represses transcription of *ompT* to achieve full colonization fitness (Provenzano and Klose, 2000). Another surface modulation of *V. cholerae* was described for this transitory step, wherein the addition of (di)glycine residues to the lipid A anchor of LPS conferred resistance to cationic antimicrobial peptides (Hankins et al., 2012). Importantly, both *V. cholerae* surface modulations can be reconstituted *in vitro* by variations in culture conditions. Reconstitution of these processes thus allows temporal monitoring of the surface exchange in strains with differential vesiculation activity.

In this study, we used three scenarios—host entry, exposure to host defense mediators (bile and polymyxin B [PMB]), and medium-induced activation of *ToxR* and/or LPS modification—to model infection-relevant life cycle transitions for *V. cholerae*. These models were applied to monitor bacterial cell surface modulation under conditions where transporter activity and therefore vesiculation could be controlled. We show that *V. cholerae* silences the expression of the *VacJ/Yrb* transporter inside the host and reduced transporter activity facilitates

colonization fitness in the murine infection model. Our findings demonstrate that upregulated vesiculation aids adaptation to both the cationic antimicrobial peptide PMB, via fast accumulation of glycine-modified lipid A, and bile salts, via efficient removal of OmpT. Thus, this study defines a physiological role for OMV production during host colonization where cell surface variation driven by increased OM vesiculation promotes adaptation of a bacterial pathogen upon host entry.

RESULTS

Silencing of VacJ/Yrb ABC Transport System *In Vivo* Increases Colonization Fitness of *V. cholerae*

The recently established TetR-controlled recombination-based *in vivo* expression technology (TRIVET) was used to monitor transcriptional silencing of the *yrb* gene cluster in *V. cholerae* (Cakar et al., 2018). TRIVET is a highly sensitive, single-cell-based reporter technique to detect temporal gene repression by an irreversible switch of an antibiotic resistance phenotype. The system allows detection of gene repression in complex environments with a relatively low bacterial load, such as the intestinal tract. In this approach, a promoterless *tetR* allele is integrated in the *V. cholerae* chromosome under the sole control of the promoter of the gene of interest. Once produced, TetR, in turn, represses TnpR resolvase expression, which excises irreversibly an antibiotic resistance (res) cassette. In short, silencing of *tetR* will induce *tnpR* and cause an irreversible loss of the res cassette, which can be monitored by a phenotypic change of the antibiotic resistance profile. Hence, resolution frequencies inversely correlate with the expression level of the investigated gene.

Here, we integrated the *tetR* allele in the *V. cholerae* chromosome downstream of the *yrbF-B* operon promoter (Figure 1A). We then examined the resolution frequencies for the corresponding TRIVET strain Vc_res_TRIVET *yrb::tpc* grown for 22 h in Lura Bertani (LB) supplemented with either FeSO₄ or 2,2'-bipyridyl to mimic high or low iron availability, respectively, as well as during colonization of the murine intestinal tract (Figure 1B). Relatively low-resolution frequencies were detected in regular LB broth, or in LB upon addition of FeSO₄, indicating sufficient *yrb*-promoter activity to silence *tnpR*. In agreement with previous results (Roier et al., 2016), resolution levels were significantly increased in LB broth supplemented with the iron chelator 2,2'-bipyridyl, reflecting the silencing of the *yrb* genes under low iron conditions.

High-resolution frequencies *in vivo* were also observed during colonization of the mouse intestine 6 and 22 h post-infection (Figure 1B). *In vivo* repression of *yrbE* and *vacJ* was independently confirmed by quantitative real-time PCR (Figure S1). Overall, the results indicate a significant repression of the *yrbF-B* operon at early stages of the infection compared with growth in regular LB broth. Based on the current model, inactivation or downregulation of the VacJ/Yrb transporter system results in phospholipid accumulation in the OM promoting OMV release (Figure 1A) (Roier et al., 2016). Concordantly, deletion of *yrbE*, encoding the permease unit of the VacJ/Yrb transport system, resulted in a hypervesiculating $\Delta yrbE$ mutant (Figure 1C). Expression of *yrbE* *in trans* ($\Delta yrbE$ pyr*bE*) reduced the hypervesiculation compared with a $\Delta yrbE$ mutant carrying the empty vector ($\Delta yrbE$ p) (Figure 1C). In contrast, reduced vesiculation

(hypovesiculation) was achieved upon overexpression of the *yrbF-B* operon from an isopropyl β -D-1-thiogalactopyranoside (IPTG)-inducible plasmid in WT (WT pyr*bF-B*) compared to the wild type (WT) carrying the empty vector (WT p) (Figure 1C). Notably, derivatives of this plasmid allow expression even in the absence of IPTG and have been used extensively for *V. cholerae* studies *in vivo* (Tamayo et al., 2008; Schild et al., 2007; Butler and Camilli, 2004; Osorio et al., 2004). However, stable plasmid maintenance requires antibiotic selection, which has been reported to elevate OMV levels in bacteria, including *V. cholerae* (Figure 1C) (Bauwens et al., 2017; Roier et al., 2016). To avoid this effect of antibiotic use, a complementation strain (*yrbE*^{*}) was constructed by reconstitution of a slightly modified *yrbE* allele in $\Delta yrbE$ on the chromosome (described in STAR Methods). The *yrbE*^{*} complementation strain not only showed significantly reduced vesiculation levels compared with $\Delta yrbE$ but also similar vesiculation levels compared with the WT (Figure 1C). Thus, *yrbE*^{*} was chosen for complementation assays throughout this study.

We next investigated the impact of vesiculation on colonization fitness. The $\Delta yrbE$ mutant and WT overexpressing the *yrbF-B* operon (WT pyr*bF-B*) were challenged, respectively, in a competition assay with a fully virulent LacZ⁻ derivative of the WT (WT^{lacZ-}) or WT carrying the empty vector (WT^{lacZ-} p), in LB broth (*in vitro*) and *in vivo* using the infant mouse model. Compared with the *in vitro* control assay, the hypervesiculating $\Delta yrbE$ mutant exhibited a significant advantage over the WT during intestinal colonization (Figure 1D). In contrast, the hypovesiculating WT pyr*bF-B* was significantly attenuated *in vivo* compared with the WT^{lacZ-} p (Figure 1D). Differential loss of the empty vector (p) and expression vector (pyr*bF-B*) can be excluded as p and pyr*bF-B* are maintained at comparable levels during *in vitro* cultivation and *in vivo* colonization (Figure S1B). Thus, increased vesiculation correlates directly with enhanced colonization fitness in the murine model.

Hypervesiculation Facilitates Exchange of OM Structures during Transition Stages

A recent report indicated that OMV release allows for the selective loss of certain LPS species from the OM of *Salmonella* following pH shifts (Bonnington and Kuehn, 2016). Likewise, the observed fitness advantage of hypervesiculating *V. cholerae* strains might be at least partially explained by alteration of the cell surface via enhanced OMV release upon host entry. In *V. cholerae*, two adaptive surface modulations occurring in the host environment have been reported: (1) removal of the OM porin OmpT to confer bile resistance (Provenzano and Klose, 2000) and (2) accumulation of (di)glycine-modified lipid A to increase resistance to cationic antimicrobial peptides (Hankins et al., 2012). We aimed to establish a system for inducing each of these surface modifications *in vitro* to subsequently analyze the impact of vesiculation on the remodeling efficacy. Fortunately, the regulatory pathways and key players for both surface modulations are known and include the virulence gene regulator ToxR, which inversely controls *ompU* and *ompT* expression, as well as the aminoacyl lipid modification (Alm) pathway required for (di)glycation of lipid A (Hankins et al., 2012; Provenzano and Klose, 2000).

Previous work indicated that cultivation in minimal media plus the four amino acids asparagine, arginine, glutamate, and serine

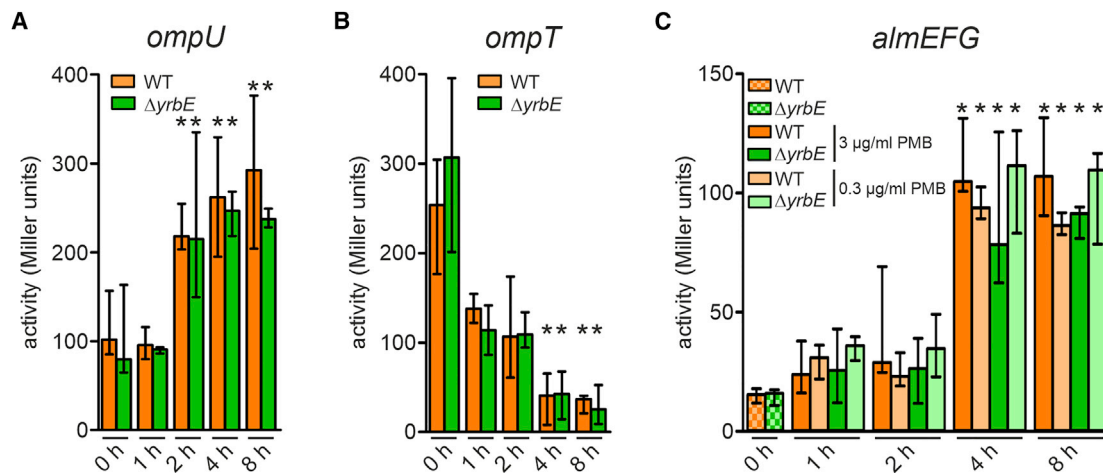


Figure 2. Differential Expression of *almG*, *ompU*, and *ompT* in a Transition from Minimal Media M9 to M9^{ToxR1} or M9^{ToxR1/Alm1}

(A and B) Alkaline phosphatase activities of WT and $\Delta yrbE$ harboring an *ompU*-*phoA* transcriptional fusion (A) and *ompT*-*phoA* transcriptional fusion (B) in M9 (0 h) as well as 1, 2, 4, and 8 h after the transition to M9^{ToxR1}. Data presented are median \pm IQR with the following number of biological replicates: in the case of *ompU*-*phoA* (A), $n = 17$ for WT at 0 h; $n = 10$ for $\Delta yrbE$ at 0 h; $n = 4$ for WT at 1, 2, 4, and 8 h; and $n = 6$ for $\Delta yrbE$ at 1, 2, 4, and 8 h, and in the case of *ompT*-*phoA* (B), $n = 9$ for WT and $\Delta yrbE$ at 0 h; $n = 6$ for WT and $\Delta yrbE$ at 1 h; and $n = 4$ for WT and $\Delta yrbE$ at 2, 4, and 8 h.

(C) Alkaline phosphatase activities of WT and $\Delta yrbE$ harboring an *almG*-*phoA* transcriptional fusion in M9 as well as 1, 2, 4, and 8 h after transition to M9^{ToxR1/Alm1} (including either 3 or 0.3 $\mu\text{g}/\text{mL}$ final PMB concentrations as indicated). Data presented are median \pm IQR with the following number of biological replicates: $n = 4$ for WT (0 and 2 h with 3 $\mu\text{g}/\text{mL}$ PMB) and $\Delta yrbE$ (0 h); $n = 8$ for WT (1 and 4 h with both PMB concentrations, 8 h with 0.3 $\mu\text{g}/\text{mL}$ PMB) and $\Delta yrbE$ (1 h with both PMB concentrations, 4 and 8 h with 0.3 $\mu\text{g}/\text{mL}$ PMB); $n = 5$ for WT (8 h with 3 $\mu\text{g}/\text{mL}$ PMB); and $n = 6$ for WT (2 h with 0.3 $\mu\text{g}/\text{mL}$ PMB) and $\Delta yrbE$ (2 h with 0.3 $\mu\text{g}/\text{mL}$ PMB, 4 and 8 h with 3 $\mu\text{g}/\text{mL}$ PMB).

(A–C) Significant differences along the transition (1 to 8 h) to the respective 0 h time points are indicated by an asterisk (* $p < 0.05$).

(NRES) significantly increases ToxR levels, resulting in the activation of *ompU* and repression of *ompT* (Mey et al., 2012). To validate differential regulation in our experimental setup, we measured alkaline phosphatase (PhoA) activities in *ompU*-*phoA* and *ompT*-*phoA* reporter strains harboring a transcriptional fusion of the promoterless *phoA* to the *ompU* or *ompT* promoters (Figures 2A and 2B). Upon transition from minimal medium M9 to M9 supplemented with NRES (M9^{ToxR1}), a significant increase in PhoA activity for *ompU*-*phoA* reporter strains was observed, whereas *ompT*-*phoA* reporter strains exhibited a significant decrease (Figures 2A and 2B). Thus, the ToxR-dependent OmpU/T switch can also be activated *in vitro* by shifting *V. cholerae* from M9 to M9^{ToxR1}.

The LPS modification system responsible for the addition of (di)glycine residues to lipid A during *de novo* synthesis at the cytoplasmic side of the inner membrane is encoded by the operon *almEFG* (Hankins et al., 2012). The Alm pathway can be activated in the presence of sublethal concentrations of cationic antimicrobial peptides (Herrera et al., 2014). To validate *almEFG* induction in our setup, we constructed reporter strains harboring a transcriptional fusion of the promoterless *phoA* to the *almEFG* promoter. Concordant with previous reports (Herrera et al., 2014), we measured a significant increase in PhoA activity upon growth in M9^{ToxR1} with sub-growth inhibitory concentrations of PMB (M9^{ToxR1/Alm1}) compared with M9 (Figure 2C). Notably, comparable temporal induction and maximum levels are observed with 0.3 and 3 $\mu\text{g}/\text{mL}$ PMB, the two concentrations used throughout this study to activate the Alm pathway. This suggests that both PMB concentrations have a similar potential to activate the Alm pathway. We conclude that both

surface modulations can be activated *in vitro* on the WT and $\Delta yrbE$ background using minimal media M9 with supplements: (1) the OmpU/T switch is activated via cultivation in M9^{ToxR1} allowing bile adaptation, and (2) presence of PMB (M9^{ToxR1/Alm1}) additionally activates the Alm pathway, allowing adaptation to cationic antimicrobial peptides.

To investigate whether differential vesiculation affects the dynamics of the surface exchange, regular and hypervesiculating *V. cholerae* strains were shifted from minimal medium M9 to M9^{ToxR1/Alm1}, and samples were collected over time. Analysis of the transcriptional expression pattern of the *almEFG* operon along the shift experiment showed that induction takes approximately 4 h (Figure 2C). Therefore, we obtained lipid A extracts of the WT, hypervesiculating $\Delta yrbE$, and *yrbE** complementation strain for liquid chromatography-mass spectrometry (LC-MS) analyses at 0, 4, 6, and 8 h after the M9 to M9^{ToxR1/Alm1} shift. The lipid A species were detected as doubly charged ions with m/z 877.7 for the unmodified lipid A (U), 906.2 for mono-glycinated lipid A (M1), and 934.7 for di-glycinated lipid A (M2) species. The peaks of these three species (U, M1, and M2) are shown in the corresponding extracted ion chromatograms (Figure 3). At 0 h, peaks reflecting the U species were readily detected in all strains, while the (di)glycine-modified lipid A species were below the limit of detection. At 4 h post-medium shift, peaks reflecting the M1 were already prevalent in hypervesiculating $\Delta yrbE$ mutant extracts but only a minor population in the WT or still below the limit of detection in the *yrbE** complementation strain (Figure 3). At 6 h post-medium shift, peaks reflecting the (di)glycine-modified lipid A species dominated in the hypervesiculating $\Delta yrbE$ mutant extracts, whereas only a minor

fraction was modified in WT and *yrbE*^{*}. However, the extent of surface modulation in the WT still increased at later time points to finally reach a similar abundance of the unmodified and (di)glycine-modified lipid A species at 8 h after the medium shift. In general, the *yrbE*^{*} complementation strain showed the lowest prevalence of (di)glycine-modified lipid A species with U species dominating even at the 8 h time point. Extracts from a Δ *almG* mutant isolated at the same 8 h time point served as a negative control and lacked peaks reflecting (di)glycine-modified lipid A, as expected (Figure S2).

We conclude that exposure to sub-growth inhibitory concentrations of PMB caused Δ *yrbE* and WT to accumulate (di)glycine-modified lipid A in the OM in an Alm-dependent manner, but the hypervesiculating Δ *yrbE* displayed the surface modification more rapidly (Figure 3). A comparison of the activities obtained using the chromosomal *almG-phoA* reporter fusions generated in the Δ *yrbE* and WT backgrounds (Figure 2C) allowed us to exclude differential expression levels or altered regulation of *alm* genes during the induced transition as a possible explanation for this accelerated modulation of the hypervesiculating mutant. As expected, PhoA levels in the WT and Δ *yrbE* background were relatively low in M9 but increased comparably for both strains throughout the shift experiment (Figure 2C). Thus, the most likely scenario explaining the faster accumulation of modified lipid A in the hypervesiculating Δ *yrbE* is an enhanced surface turnover due to increased vesiculation, resulting in faster depletion of U from the OM.

We then monitored OmpT depletion in whole-cell lysates or OM preparations for the WT, hypervesiculating Δ *yrbE*, and *yrbE*^{*} complementation strain in response to the M9 to M9^{ToxR \uparrow} shift as a model for the adaptational response to bile. Immunoblot analyses revealed that OmpU increased slightly over time in whole-cell lysates or remained at stable high levels at all time points sampled in OM preparations for all strains (Figure 4). The increase observed in whole-cell lysates follows the activation of *ompU* expression during the shift experiment (Figure 2A). Increasing OmpU might not be visible in OM preparations as these samples were normalized to protein equivalents, which can be seen as an adjustment to the most abundant protein, namely OmpU (Chakrabarti et al., 1996). In contrast to OmpU, OmpT was depleted in whole-cell lysates and from the OM preparations for all strains during the transition (Figure 4). We verified that equal amounts of protein were loaded in all lanes by Coomassie-stained SDS gels (Figure S3) and additionally by immunodetection of the α -subunit of the RNA Polymerase (RpoA) in whole-cell lysates (Figure 4). Notably, the rate of OmpT depletion differed between strains. In the WT and *yrbE*^{*} complementation strain, a marked reduction of OmpT signal intensity was observed from 4 h onward, while OmpT loss was detected after 1 h in the hypervesiculating Δ *yrbE* strain (Figure 4). In line with the AlmEFG expression profile, the temporal regulation of *ompT* and *ompU* expression during the shift experiment is similar in WT and Δ *yrbE* (Figures 2A and 2B), excluding differential regulation in the two strains.

To evaluate a direct role for vesiculation in the OmpU/T switch, OMVs were isolated from culture supernatants obtained at 0, 4, and 8 h of the transition experiment, and the relative abundance of these proteins was compared (Figure 4). OmpT appeared already at 4 h in OMVs released by Δ *yrbE* but only after 8 h in the OMVs derived from WT and *yrbE*^{*}. Hence, the most likely explanation for the OM depletion of OmpT along the transition is a constant removal of OmpT and other components via vesiculation, combined with transcriptional repression of *ompT* and *de novo* synthesis. In summary, the adaptive depletion of OmpT from the OM of *V. cholerae* can be linked to its deposition into OMVs. The hypervesiculating Δ *yrbE* mutant is thus able to more rapidly discharge OmpT from its OM. In conclusion, both adaptive surface modulations tested here were implemented more rapidly in the hypervesiculating Δ *yrbE* mutant than in a normally vesiculating WT strain.

Hypervesiculation Facilitates Faster Adaptation to the Cationic Antimicrobial Peptide PMB during Transition Stages

As previously reported, accumulation of (di)glycine-modified lipid A facilitates bacterial survival in the presence of cationic antimicrobial peptides, while depletion of OmpT from the OM promotes resistance to bile (Hankins et al., 2012; Provenzano and Klose, 2000). We hypothesized that the faster accumulation of (di)glycine-modified lipid A as well as removal of OmpT observed in a hypervesiculating strain correlates with faster adaptation to these host defenses. To test this premise, we asked whether strains with differential vesiculation exhibit different sensitivity to PMB and bile.

First, the minimal inhibitory concentration (MIC) of PMB affecting growth of the hypervesiculating Δ *yrbE* mutant and regular vesiculating WT was assessed for the transition from M9 to M9^{ToxR \uparrow /Alm \uparrow} as a model for the adaptation phase early in infection. To this end, overnight cultures of the Δ *yrbE* mutant and WT grown in M9 were allowed to adapt for 2 h in M9^{ToxR \uparrow /Alm \uparrow} ((di)glycine-modified lipid A activating conditions using sub-minimal inhibitory concentrations [MIC] PMB [3 μ g/mL]) before additional PMB was added to achieve inhibitory concentrations. A 2-h adaptation phase was chosen, as it closely reflects the dynamics of a natural *V. cholerae* infection, i.e., it reflects the time from oral ingestion to arrival of the bacteria at their primary colonization site in the small intestine (Angelichio et al., 1999). A significantly higher MIC was obtained for the hypervesiculating Δ *yrbE* mutant than WT, implying stronger resistance and better adaptation to PMB (Figure 5A). A transition of the same M9 overnight cultures to M9 failed to activate the Alm pathway. As expected under these conditions, Δ *yrbE* and WT exhibited comparably poor resistance to PMB indicated by equally low MIC values (Figure 5A). Conversely, overnight cultures grown in M9^{ToxR \uparrow /Alm \uparrow} shifted to M9^{ToxR \uparrow /Alm \uparrow} served as fully adapted controls. Accordingly, equally high MIC values were obtained

strain and time point. At the bottom, chemical structures and formulas of the three lipid A species U, M1, and M2 (according to Hankins et al. [2012]), including the high-resolution mass spectra of the doubly charged lipid A species with their isotope patterns, are shown. See also Figure S2.

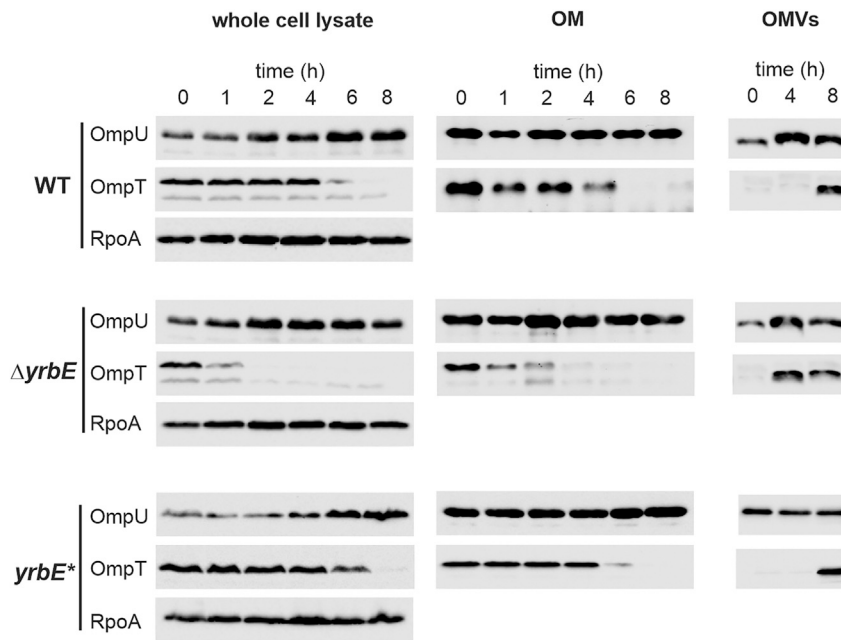


Figure 4. Vesiculation Accelerates Depletion of OmpT from the OM

Samples of whole-cell lysates, OM preparations, and OMVs were isolated from WT, $\Delta yrbE$, and $yrbE^*$ at times indicated after the transition from minimal medium M9 to M9^{ToxR1}. Equivalent amounts of total proteins were resolved electrophoretically, and representative immunoblots detected OmpU, OmpT, and RpoA in the case of whole-cell lysates (left) or OmpU and OmpT in the case of OM preparations (center) and OMVs (right). Coomassie-stained SDS gels executed in parallel additionally controlled loading of equal protein amounts in all lanes.

See also Figure S3.

for the $\Delta yrbE$ mutant and WT. Thus, the hypervesiculating strains have no advantage in non-adapted or fully adapted stages but only transiently during the adaptation phase (Figure 5A). To link the observed advantage to the lipid A modification, we performed the experiment in an $\Delta almG$ background. Although deletion of $yrbE$ in an $\Delta almG$ background still resulted in an hypervesiculating phenotype (Figure S4A), the MICs of PMB were similar for the normally vesiculating $\Delta almG$ and the hypervesiculating $\Delta almG\Delta yrbE$ following the M9 to M9^{ToxR1/Alm1} transition (Figure S4B). Notably, a lower adaptive PMB concentration (0.3 instead of 3 $\mu\text{g}/\text{mL}$) had to be used for $\Delta almG$ and $\Delta almG\Delta yrbE$ than for the other strains to accommodate the previously reported lower PMB resistance of alm mutants compared with WT (Hankins et al., 2012). Nonetheless, we observed earlier that induction of the Alm pathway was similar for 0.3 and 3 $\mu\text{g}/\text{mL}$ PMB (Figure 2C), indicating that both PMB concentrations have a comparable potential to activate the Alm pathway. Thus, the transient advantage of the hypervesiculating strain in the PMB adaptation is AlmG dependent.

We next compared the survival fitness of WT, $\Delta yrbE$, and $yrbE^*$ exposed to a sub-MIC PMB concentration (3 $\mu\text{g}/\text{mL}$) present in M9^{ToxR1/Alm1}. Bacterial cultures were grown and shifted using the M9 and M9^{ToxR1/Alm1} model as described above. Upon transition, cell viability dropped massively with equally low survival rates of approximately 1% obtained for all strains at 2 and 4 h (Figure 5B). At 8 h, average survival rates increased for all strains tested, suggesting adaptation to PMB. However, survival rates of $\Delta yrbE$ were significantly higher than that for WT and $yrbE^*$, highlighting an advantage for the hypervesiculating strain. After 24 h, all strains had proliferated to a similar extent, exceeding the starting colony-forming unit (CFU). Moreover, growth upon transition from M9 to M9^{ToxR1/Alm1} was analyzed to visualize the differential adaptation dynamics. After a relatively long lag phase, the hypervesiculating $\Delta yrbE$ entered into exponential

growth about 2 h earlier than the WT (Figure 5C). Accordingly, the area under the curve (AUC), reflecting the overall biomass produced within the observed time, was significantly higher for the hypervesiculating $\Delta yrbE$ than that for WT (Figure 5D). Similar growth was observed for all strains used in these assays if bacteria were

shifted from M9 to M9^{ToxR1} in the absence of PMB (Figures S5A and S5B). Thus, a general growth advantage of $\Delta yrbE$ can be excluded.

Hypervesiculation Facilitates Faster Adaptation to Bile Salts during Transition Stages

Next, we asked whether the faster removal of OmpT from the OM mediated by hypervesiculation promotes a more rapid adaptation to bile. Unexpectedly, the deletion mutant $\Delta yrbE$ was 3-fold more sensitive to bile compared with WT or $yrbE^*$ in M9 (Figure S6A). All three strains exhibited comparable sensitivity to PMB and SDS treatment, which excludes a general defect in the OM integrity upon hypervesiculation (Figures 5A and S6B). Characterization of the previous loss-of-function mutations of the VacJ/Yrb transporter, however, provided a possible explanation. The complete loss of the retrograde lipid trafficking resulted in excessive amounts of phospholipids in the OM (Roier et al., 2016). The normal lipid asymmetry of the OM was lost as a result, and large patches of phospholipid bilayers appeared (Mallinverni and Silhavy, 2009; Roier et al., 2016). Importantly, bile penetrates such phospholipid bilayers more effectively than asymmetric OMs composed of an LPS and phospholipid leaflet (Benz and Bauer, 1988; Hancock, 1984) and may therefore account for increased sensitivity of the $\Delta yrbE$ mutant to bile.

To overcome this limitation, a strain allowing finer control of the yrb genes was constructed. The chromosomal promoter of the yrb operon was replaced by an arabinose-inducible promoter strain, and the corresponding regulator $araC$ was inserted into the $lacZ$ locus generating the arabinose-inducible strain $yrbF-B^{\text{PARA}}$. This allowed a controllable expression of the yrb genes. Basal expression levels in the absence of arabinose and increased production in the presence of arabinose was confirmed by quantitative real-time PCR (Figure S6C). Accordingly, OMV production by a $yrbF-B^{\text{PARA}}$ culture was low when grown in M9^{ToxR1} with arabinose and significantly higher in

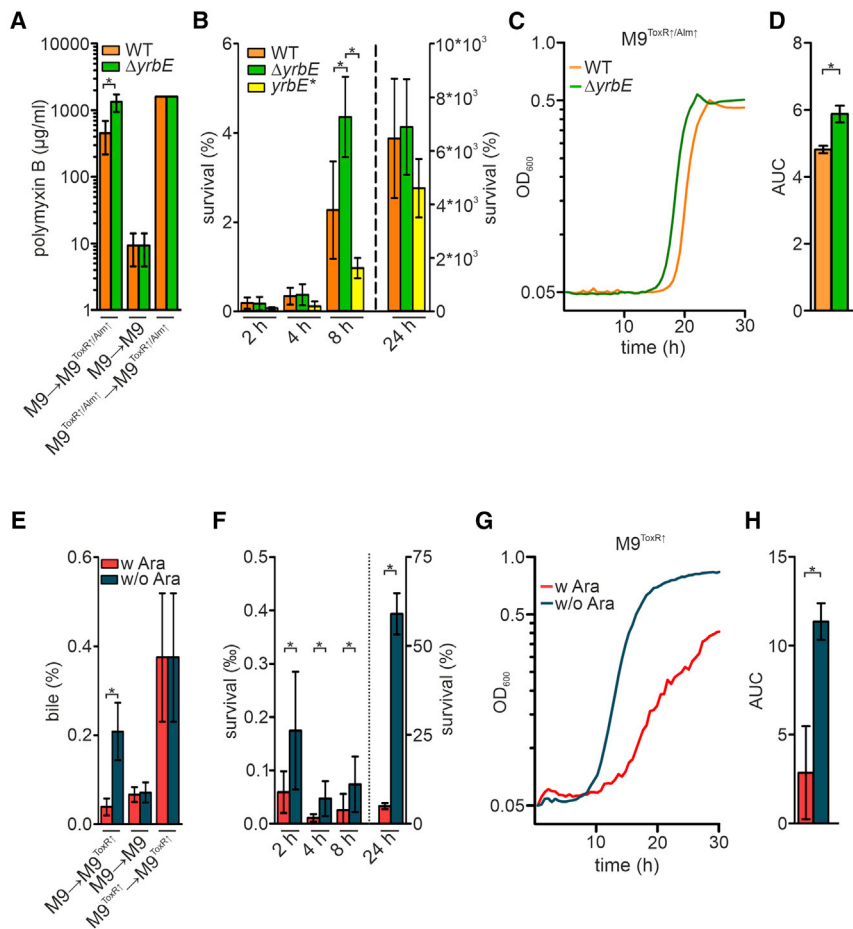


Figure 5. Enhanced Vesiculation Facilitates Adaptation to PMB and Bile upon Transition from M9 to M9^{ToxR1/Alm1} or M9^{ToxR1}

(A) Minimal inhibitory concentrations (MIC) of PMB for WT and $\Delta yrbE$ after a M9 to M9^{ToxR1/Alm1}, M9 to M9, or M9^{ToxR1/Alm1} to M9^{ToxR1/Alm1} transition. Bacteria were allowed to adapt for 2 h after transition into fresh medium before (additional) PMB was added to achieve diverse concentrations for MIC-determination. Data presented are mean \pm standard deviation (SD) with the following number of biological replicates for WT and $\Delta yrbE$: n = 11 for the M9 to M9^{ToxR1/Alm1} transition and n = 6 for the M9 to M9 and M9^{ToxR1/Alm1} to M9^{ToxR1/Alm1} transition.

(B) Survival of WT, $\Delta yrbE$, and $yrbE^*$ was determined by CFU plating along the M9 to M9^{ToxR1/Alm1} (including sub-MIC concentrations of PMB [3 μ g/mL]) transition at 2, 4, 8, and 24 h. Data presented are mean \pm SD with the following number of biological replicates: n = 18 for WT at 2 and 4 h; n = 10 for $\Delta yrbE$ at 2 and 4 h; n = 8 for $yrbE^*$ at 2, 4, and 8 h; n = 14 for WT at 8 h; n = 6 for $\Delta yrbE$ at 8 and 24 h and $yrbE^*$ at 24 h.

(C) Growth curves reporting mean values (n = 6) of WT and $\Delta yrbE$ upon transition from M9 to M9^{ToxR1/Alm1} (including sub-MIC concentrations of PMB [3 μ g/mL]).

(D) Mean area under the curve (AUC) values \pm SD retrieved from the growth curves presented in (C) (n = 6).

(E) MIC of bile for the arabinose-inducible strain $yrbF-B^{pARA}$ after a M9 to M9^{ToxR1}, M9 to M9, or M9^{ToxR1} to M9^{ToxR1} transition with (W) or without (W/O) arabinose (Ara). Overnight cultures were always grown in the presence of arabinose and allowed to adapt for 2 h after transition into the fresh medium (M9 or M9^{ToxR1} as indicated). After the 2-h adaptation phase, differential amounts of bile were

added to determine the MIC. Data presented are mean \pm SD with the following number of biological replicates for $yrbF-B^{pARA}$ W and W/O Ara: n = 6 for the M9 to M9^{ToxR1} transition, n = 14 for the M9 to M9 transition, and n = 4 for the M9^{ToxR1} to M9^{ToxR1} transition.

(F) Survival of the arabinose-inducible strain $yrbF-B^{pARA}$ was determined by CFU plating along the M9 to M9^{ToxR1} transition W or W/O Ara at 2, 4, 8, and 24 h in the presence of sub-MIC bile concentrations (0.1%). Data presented are mean \pm SD with the following biological replicates for $yrbF-B^{pARA}$ W and W/O Ara: n = 4 for 24 h and n = 8 for all other time points.

(G) Growth curves reporting mean values (n = 6) of the arabinose-inducible strain $yrbF-B^{pARA}$ upon transition from M9 to M9^{ToxR1} W or W/O Ara in the presence of sub-MIC bile concentrations (0.1%).

(H) Mean AUC values \pm SD retrieved from the growth curves presented in (G) (n = 6).

(A–H) Significant differences are indicated by an asterisk (*p < 0.05).

See also [Figures S4–S6](#).

M9^{ToxR1} lacking arabinose (Figure S6C). The $yrbF-B^{pARA}$ strain thus allowed us to assess the dynamics of vesiculation upon silencing of the *yrb* operon. Already, 4 h after the depletion of arabinose, a small but significant increase in vesiculation could be detected in comparison to a culture grown in the presence of arabinose (Figure S6C). Notably, the highest vesiculation levels achieved for $yrbF-B^{pARA}$ in the absence of arabinose were still 2-fold lower than that for the loss-of-function mutant $\Delta yrbE$ (Figures 1C and S6C), indicating a basal *yrb* operon expression level in $yrbF-B^{pARA}$ even in the absence of arabinose. Strain $yrbF-B^{pARA}$ followed the same principles as the regular vesiculating WT and hypervesiculating $\Delta yrbE$ mutant for the adaptation to PMB upon shift to M9^{ToxR1/Alm1} (Figures 5A and S6D). Consistent with the results obtained for WT and $\Delta yrbE$, a higher MIC of PMB was observed for strain $yrbF-B^{pARA}$ under high vesiculation conditions (no arabinose) compared with low

vesiculation cultivation (with arabinose). Most importantly, a similar sensitivity to bile was observed for $yrbF-B^{pARA}$ grown in M9 with and without arabinose (Figure 5E). Thus, the strain $yrbF-B^{pARA}$ is perfectly suited to analyze the impact of differential vesiculation on bile adaptation during transition events.

In general, bile adaptation experiments using the strain $yrbF-B^{pARA}$ in the presence or absence of arabinose followed the design described above for the PMB resistance mediated by accumulation of (di)glycine-modified lipid A (Figure 5). Overnight cultures of the strain $yrbF-B^{pARA}$ were grown in M9 or M9^{ToxR1} in the presence of arabinose to promote expression of the *yrb* genes, resulting in moderate vesiculation levels. Subsequently, overnight cultures were shifted from M9 to M9^{ToxR1} with or without arabinose (inducing ToxR-dependent *ompT* repression), from M9 to M9 with or without arabinose (no *ompT* repression) or M9^{ToxR1} to M9^{ToxR1} with or without arabinose

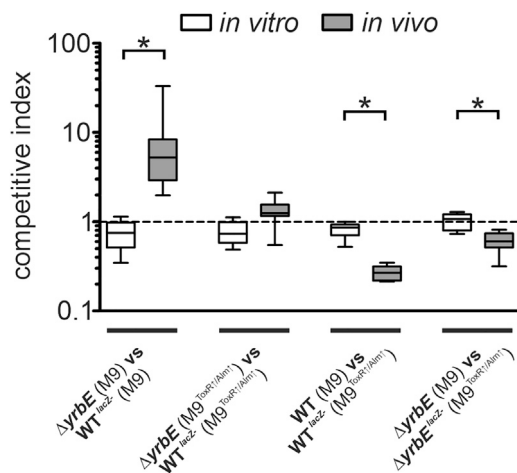


Figure 6. Colonization Advantage of the Hypervesiculating Strain Is Compensated by Pre-adaptation to Bile and PMB

Competition assays were performed *in vitro* (M9) and *in vivo* (murine model) between the WT or the hypervesiculating $\Delta yrbE$ mutant against their isogenic $lacZ^-$ derivatives (WT^{lacZ^-} or $\Delta yrbE^{lacZ^-}$). Strains as well as the cultivation conditions of the inoculum used for the competition are indicated on the x axis. The data are presented as a boxplot with whiskers (* $p < 0.05$) with the following number of biological replicates: $n = 8$ for *in vitro* competitions of WT^{lacZ^-} versus $\Delta yrbE$; $n = 9$ for *in vivo* competitions of WT^{lacZ^-} versus $\Delta yrbE$ grown in M9; $n = 10$ for *in vivo* competitions of WT^{lacZ^-} versus $\Delta yrbE$ in $M9^{ToxR\uparrow/Alm\uparrow}$; $n = 12$ for *in vitro* competitions of WT versus WT^{lacZ^-} and $\Delta yrbE$ versus $\Delta yrbE^{lacZ^-}$; and $n = 7$ for *in vivo* competitions of WT versus WT^{lacZ^-} and $\Delta yrbE$ versus $\Delta yrbE^{lacZ^-}$.

(ToxR-dependent *ompT* repression already in the overnight culture). The presence or absence of arabinose triggered moderate or increased vesiculation. Consistent with the PMB transition assays, bacteria were allowed to adapt for 2 h after transition into the fresh media before different bile concentrations were added.

In the M9 to $M9^{ToxR\uparrow}$ transition experiment, significantly higher MIC values for bile were obtained with the strain grown in the absence of arabinose reflecting hypervesiculation than the moderately vesiculating strain grown with arabinose. This finding links increased vesiculation with higher resistance levels along the transition and better adaptation to bile (Figure 5E), which is in very good agreement with the PMB adaptation data. A M9 to M9 transition prevented the *ompT* silencing and served as a control. Consequently, equally low MIC values were observed in the assays regardless of the presence or absence of arabinose (Figure 5E). Conversely, overnight cultures grown in $M9^{ToxR\uparrow}$ shifted into $M9^{ToxR\uparrow}$ with or without arabinose served as controls with full adaptation to bile achieved before the transfer resulting in equally high MIC values (Figure 5E).

To assess temporal survival in the presence of bile, the strain $yrbF-B^{pARA}$ was grown overnight in M9 with arabinose and shifted to $M9^{ToxR\uparrow}$ with or without arabinose for 2 h before a sub-MIC bile concentration (0.1%) was added. Generally, a severe drop in survival rates below 1% could be observed. Survival reached a minimum at around 4 h and then rose again afterward (Figure 5F). Notably, the survival rates of the hypervesiculating strain (no arabinose) were significantly higher than the lower vesiculating strain for all time points (Figure 5F).

Finally, growth curves in the presence of a sub-MIC bile concentration (0.1%) were created to visualize the differential adaptation dynamics (Figure 5G). Again, the hypervesiculating strain without arabinose entered earlier into the exponential phase and showed more robust proliferation compared with the lower vesiculating strain grown with arabinose. This advantage is also indicated by AUC values, which were significantly higher for the strain grown in the absence of arabinose than in the presence of arabinose (Figure 5H). Similar growth was observed in $M9^{ToxR\uparrow}$ with and without arabinose (Figures S5C and S5D), excluding an arabinose-dependent growth difference of strain $yrbF-B^{pARA}$.

Pre-adaptation to Bile and PMB Negates *In Vivo* Advantage of a Hypervesiculating Strain

Our data support the model that the faster exchange of cell surface composition observed for hypervesiculating strains is associated with a faster adaptation to antimicrobial compounds. We therefore asked next whether this mechanism underlies the *in vivo* fitness advantage of hypervesiculating strains. If true, the colonization advantage of a hypervesiculating strain should be diminished if fully adapted strains are used for the *in vivo* competition experiments. We took advantage of the fact that growth overnight in $M9^{ToxR\uparrow/Alm\uparrow}$ activates both infection-relevant surface modulations studied thus far. Equally high resistance levels to antibacterial challenge *in vitro* indicated full adaptation of moderate and hypervesiculating strains (Figures 5A and 5E). The *in vivo* competition assays were then performed using inocula of the hypervesiculating $\Delta yrbE$ mutant and normally vesiculating WT that had been grown in M9 (no adaptation) or $M9^{ToxR\uparrow/Alm\uparrow}$ (full adaptation). As observed for LB cultures (Figure 1D), the hypervesiculating strain still outcompeted the WT *in vivo* when the inoculum was derived from M9 cultures (Figure 6). In contrast, $\Delta yrbE$ and WT competed equally well in the murine model when the inoculum was derived from $M9^{ToxR\uparrow/Alm\uparrow}$ cultures. Moreover, non-adapted WT (grown in M9) was approximately 4-fold attenuated *in vivo* compared with an adapted WT (grown in $M9^{ToxR\uparrow/Alm\uparrow}$), whereas a non-adapted $\Delta yrbE$ (grown in M9) was only 2-fold attenuated *in vivo* compared with an adapted $\Delta yrbE$ (grown in $M9^{ToxR\uparrow/Alm\uparrow}$). Thus, non-adapted strains are generally attenuated compared with their adapted counterparts, but hypervesiculation can partially compensate this disadvantage. Hence, we conclude that the *in vivo* advantage of hypervesiculating strains at early stages of infection is due to accelerated surface modulation, thus promoting adaptation to antimicrobial stressors in the intestine.

DISCUSSION

This study provides insights into the adaptation strategies of the bacterial pathogen *V. cholerae* along the environment to host transition. We characterize OMVs as a tool for OM exchange facilitating *V. cholerae*'s adaptation to antimicrobial intestinal stressors upon host entry.

Upon ingestion by the host, *V. cholerae* silences the VacJ/Yrb retrograde lipid trafficking system, which results in increased OMV release. In accordance with previous reports and data presented here, iron limitation is a likely signal for the repression of the well-conserved *vacJ* and *yrb* genes (Roier et al., 2016). Notably,

iron limitation—or nutrient limitation in general—could have been a driving evolutionary trigger for OMV release. OMV production generally increases during starvation conditions. Moreover, iron-scavenging proteins have been found in vesicles from several bacterial pathogens, which might imply a role of OMVs in iron acquisition (Gui et al., 2016; Lappann et al., 2013; Lin et al., 2017).

Coming from an aquatic lifestyle, *V. cholerae* needs to quickly change its expression profile in order to adapt to the conditions faced in the intestinal tract of the host. Besides activation of colonization factors and toxins, the adaptation to antimicrobial effectors is crucial for *V. cholerae* to achieve full virulence. The adaptation processes to cationic antimicrobial peptides and bile require changes in the OM profile, i.e., accumulation of (di)glycine-modified lipid A in LPS molecules and removal of OmpT (Hankins et al., 2011; Provenzano and Klose, 2000). Indeed, regulatory cascades driving both surface modulations are immediately activated upon host entry. Low levels of cationic antimicrobial peptides induce transcription of the AlmEFG system, which catalyzes the (di)glycine modification along *de novo* synthesis of LPS (Matson et al., 2017). Moreover, host entry activates ToxR and downregulates *ompT* transcription (Li et al., 2000; Miller and Mekalanos, 1988). Nonetheless, the time elapsed until such transcriptional changes are manifest in OM alterations can be critical. This is especially true during early stages of the infection when bacterial proliferation is rather low. Besides preventing new OmpT production and activation of (di)glycine-modified LPS synthesis, it is crucial for *V. cholerae* to deplete disadvantageous structures from the surface. OMVs provide an efficient tool to discharge unfavorable OM compounds, including proteins such as OmpT and polysaccharides such as unmodified LPS. Increased vesiculation *in vivo* not only enhances the removal of factors detrimental for colonization but also creates new space for beneficial compounds. As demonstrated in this study, hypervesiculation of *V. cholerae* allows an efficient exchange of the surface profile, facilitating the adaptation process to cationic antimicrobial peptides and bile along the environment to host transition. The importance of this adaptation is highlighted by the observation that hypervesiculation is associated with increased colonization fitness, whereas hypovesiculation results in reduced *in vivo* fitness.

Notably, increased vesiculation only provides a transient advantage during the adaptation process. Once the surface profile change is completed, the advantage of hypervesiculation is lost. Previous reports indicate that increased OMV production in *E. coli* correlates with better bacterial survival in the presence of antimicrobial agents (Kulkarni et al., 2015; Manning and Kuehn, 2011; Urashima et al., 2017). This is likely due to the fact that OMVs can act as a sink for these substances. Notably, these reports rely on OMV amounts present in fully grown cultures. To initiate the transition processes studied here, the bacterial cultures are massively diluted. Thus, the initial OMV concentrations in the survival assays of this study are very low (approximately 100-fold below the OMV amounts described to be beneficial). This difference might explain why the advantage of the hypervesiculating strain in the present study is only observed during transitions activating the surface exchange and therefore relies on the OM adaptation rather than the OMV amount.

The continuous liberation of compounds of the OM and periplasm via OMVs is highly energy consuming. Thus, it is likely

that bacteria have evolved to regulate OMV release in accordance with their needs, e.g., induction of vesiculation upon host entry. Notably, the regulation of vesiculation via transcriptional control of the VacJ/Yrb lipid trafficking system in response to iron availability seems to be conserved among diverse Gram-negative bacteria (Roier et al., 2016). Moreover, several Gram-negative pathogens modulate the OM composition upon host entry to achieve full colonization fitness. In addition to the surface modifications analyzed in this study, prominent examples include modulation of OM protein abundance involved in serum resistance (e.g., reported for *Neisseria gonorrhoeae* and *Borrelia burgdorferi*) or iron uptake (e.g., reported for *Klebsiella pneumoniae*, *Pasteurella haemolytica*, and *H. influenzae*), OM-associated proteases of *E. coli* and *Salmonella typhimurium* that degrade antimicrobial peptides, LPS modifications such as the lipid A palmitoylation (e.g., reported for *S. typhimurium*, *E. coli*, and *Yersinia enterocolitica*), the lipid A aminoarabinose modification (reported for *S. typhimurium*), and the aminoacylation of phospholipids reported for *Pseudomonas aeruginosa* contributing to antimicrobial peptide resistance (Gunn et al., 1998; Klein et al., 2009; Lin et al., 2002). Additionally, a recent *in vitro* study suggested that OMV production of *S. typhimurium* can facilitate infection-relevant LPS remodeling in the OM triggered by pH and magnesium availability (Bonnington and Kuehn, 2016). Based on these observations, we hypothesize that the surface exchange via increased vesiculation upon host entry could be a common principle of bacterial pathogens to quickly adapt to *in vivo* conditions.

Moreover, OMVs of pathogens have been reported to act as delivery vehicles of bacterial toxins and as a sink for host-derived antimicrobial factors, such as defensins and the complement system (Elluri et al., 2014; Kulp and Kuehn, 2010; Roier et al., 2016). Thus, it is becoming evident that enhanced bacterial vesicle production during host colonization can be linked to various beneficial roles, and OMVs can increase the colonization fitness of bacterial pathogens in multiple ways.

Notably, hypervesiculation is not only associated with iron availability. The VacJ/Yrb lipid trafficking system might be controlled by additional regulatory elements, and alternative OMV biogenesis mechanisms have been reported (Kulp and Kuehn, 2010). Thus, other signals may induce vesiculation, which extend the observations beyond the environment to host transition performed by the facultative human pathogen *V. cholerae*. Because production of membrane vesicles is observed for Gram-negative and Gram-positive bacteria, it is tempting to speculate that varying vesiculation levels could represent a general and efficient adaptation strategy of bacteria during transitions demanding a surface profile modulation.

STAR★METHODS

Detailed methods are provided in the online version of this paper and include the following:

- KEY RESOURCES TABLE
- LEAD CONTACT AND MATERIALS AVAILABILITY
- EXPERIMENTAL MODEL AND SUBJECT DETAILS
 - Housing Conditions for Experimental Animals
 - Competition Assay

- Resolution Assay
- Infection Studies to Obtain Bacterial RNA
- **METHOD DETAILS**
 - Bacterial Strains and Growth Conditions
 - Genetic Manipulations
 - Resolution Assay
 - Quantitative Real-time PCR
 - Isolation of Lipid A
 - Analysis of Lipid A by LC-MS
 - Preparation of OMVs
 - Preparation of Outer Membrane Proteins and Whole Cell Lysates
 - SDS-PAGE and Immunoblot
 - Growth Kinetics
 - Minimal Inhibitory Concentration (MIC)-assays
 - Survival Assays
 - Alkaline Phosphatase Assays
- **QUANTIFICATION AND STATISTICAL ANALYSIS**
- **DATA AND CODE AVAILABILITY**

SUPPLEMENTAL INFORMATION

Supplemental Information can be found online at <https://doi.org/10.1016/j.chom.2019.12.002>.

ACKNOWLEDGMENTS

We are grateful to T. Eichmann (University of Graz) for assistance with MS data evaluation, L. Schmidberger for assistance with MIC assays, and E.L. Zechner for critically reading the manuscript. This work was supported by the Bio-TechMed-Graz Flagship Project SECRETOME to S.S.; the Austrian FWF grants P25691 to S.S., P27654 to S.S., P29404 to J.R., and W901-B12 (DK Molecular Enzymology) to F.G.Z., F.C., and S.S.; as well as NIH grants AI-139105 and GM-069338 to Z.G.

AUTHOR CONTRIBUTIONS

Conceptualization, F.G.Z. and S.S.; Methodology, F.G.Z. and S.S.; Investigation, F.G.Z., P.K., F.C., D.R.L., F.M., K.E.B., G.N.R., and Z.G.; Resources, G.N.R., M.J.K., and Z.G.; Writing – Original Draft, F.G.Z.; Writing – Review & Editing, F.G.Z., F.C., K.E.B., J.R., and S.S.; Visualization, F.G.Z.; Supervision, J.R. and S.S.; Funding Acquisition, Z.G., J.R., and S.S.

DECLARATION OF INTERESTS

The authors declare no competing interests.

Received: July 17, 2019

Revised: October 25, 2019

Accepted: December 5, 2019

Published: December 31, 2019

REFERENCES

Angelichio, M.J., Spector, J., Waldor, M.K., and Camilli, A. (1999). *Vibrio cholerae* intestinal population dynamics in the suckling mouse model of infection. *Infect. Immun.* *67*, 3733–3739.

Bauwens, A., Kunsmann, L., Karch, H., Mellmann, A., and Bielaszewska, M. (2017). Antibiotic-mediated modulations of outer membrane vesicles in enterohemorrhagic *Escherichia coli* O104:H4 and O157:H7. *Antimicrob. Agents Chemother.* *61*, e00937–17.

Benz, R., and Bauer, K. (1988). Permeation of hydrophilic molecules through the outer membrane of gram-negative bacteria. Review on bacterial porins. *Eur. J. Biochem.* *176*, 1–19.

Bonnington, K.E., and Kuehn, M.J. (2016). Outer membrane vesicle production facilitates LPS remodeling and outer membrane maintenance in *Salmonella* during environmental transitions. *mBio* *7*, e01532–16.

Butler, S.M., and Camilli, A. (2004). Both chemotaxis and net motility greatly influence the infectivity of *Vibrio cholerae*. *Proc. Natl. Acad. Sci. USA* *101*, 5018–5023.

Cakar, F., Zingl, F.G., Moisi, M., Reidl, J., and Schild, S. (2018). In vivo repressed genes of *Vibrio cholerae* reveal inverse requirements of an H⁺/Cl⁻ transporter along the gastrointestinal passage. *Proc. Natl. Acad. Sci. USA* *115*, E2376–E2385.

Camilli, A., and Mekalanos, J.J. (1995). Use of recombinase gene fusions to identify *Vibrio cholerae* genes induced during infection. *Mol. Microbiol.* *18*, 671–683.

Carlone, G.M., Thomas, M.L., Rumschlag, H.S., and Sottnek, F.O. (1986). Rapid microprocedure for isolating detergent-insoluble outer membrane proteins from *Haemophilus* species. *J. Clin. Microbiol.* *24*, 330–332.

Chakrabarti, S.R., Chaudhuri, K., Sen, K., and Das, J. (1996). Porins of *Vibrio cholerae*: purification and characterization of OmpU. *J. Bacteriol.* *178*, 524–530.

Conner, J.G., Teschler, J.K., Jones, C.J., and Yildiz, F.H. (2016). Staying alive: *Vibrio cholerae*'s cycle of environmental survival, transmission, and dissemination. *Microbiol. Spectr.* *4*, <https://doi.org/10.1128/microbiolspec.VMBF-0015-2015>.

Donnenberg, M.S., and Kaper, J.B. (1991). Construction of an *aeae* deletion mutant of enteropathogenic *Escherichia coli* by using a positive-selection suicide vector. *Infect. Immun.* *59*, 4310–4317.

Elluri, S., Enow, C., Vdovikova, S., Rompikuntal, P.K., Dongre, M., Carlsson, S., Pal, A., Uhlir, B.E., and Wai, S.N. (2014). Outer membrane vesicles mediate transport of biologically active *Vibrio cholerae* cytotoxin (VCC) from *V. cholerae* strains. *PLoS One* *9*, e106731.

Fengler, V.H., Boritsch, E.C., Tutz, S., Seper, A., Ebner, H., Roier, S., Schild, S., and Reidl, J. (2012). Disulfide bond formation and ToxR activity in *Vibrio cholerae*. *PLoS One* *7*, e47756.

Gui, M.J., Dashper, S.G., Slakeski, N., Chen, Y.Y., and Reynolds, E.C. (2016). Spheres of influence: *Porphyromonas gingivalis* outer membrane vesicles. *Mol. Oral Microbiol.* *31*, 365–378.

Gumpenberger, T., Vorkapic, D., Zingl, F.G., Pressler, K., Lackner, S., Seper, A., Reidl, J., and Schild, S. (2016). Nucleoside uptake in *Vibrio cholerae* and its role in the transition fitness from host to environment. *Mol. Microbiol.* *99*, 470–483.

Gunn, J.S., Lim, K.B., Krueger, J., Kim, K., Guo, L., Hackett, M., and Miller, S.I. (1998). PmrA-PmrB-regulated genes necessary for 4-aminoarabinose lipid A modification and polymyxin resistance. *Mol. Microbiol.* *27*, 1171–1182.

Guzman, L.M., Belin, D., Carson, M.J., and Beckwith, J. (1995). Tight regulation, modulation, and high-level expression by vectors containing the arabinose PBAD promoter. *J. Bacteriol.* *177*, 4121–4130.

Hancock, R.E. (1984). Alterations in outer membrane permeability. *Annu. Rev. Microbiol.* *38*, 237–264.

Hankins, J.V., Madsen, J.A., Giles, D.K., Brodbelt, J.S., and Trent, M.S. (2012). Amino acid addition to *Vibrio cholerae* LPS establishes a link between surface remodeling in gram-positive and gram-negative bacteria. *Proc. Natl. Acad. Sci. USA* *109*, 8722–8727.

Hankins, J.V., Madsen, J.A., Giles, D.K., Childers, B.M., Klose, K.E., Brodbelt, J.S., and Trent, M.S. (2011). Elucidation of a novel *Vibrio cholerae* lipid A secondary hydroxy-acyltransferase and its role in innate immune recognition. *Mol. Microbiol.* *81*, 1313–1329.

Henderson, J.C., O'Brien, J.P., Brodbelt, J.S., and Trent, M.S. (2013). Isolation and chemical characterization of lipid A from gram-negative bacteria. *J. Vis. Exp.* *79*, e50623.

Herrera, C.M., Crofts, A.A., Henderson, J.C., Pingali, S.C., Davies, B.W., and Trent, M.S. (2014). The *Vibrio cholerae* VprA-VprB two-component system controls virulence through endotoxin modification. *mBio* *5*, e02283–14.

Hughes, G.W., Hall, S.C.L., Laxton, C.S., Sridhar, P., Mahadi, A.H., Hatton, C., Piggot, T.J., Wotherspoon, P.J., Leney, A.C., Ward, D.G., et al. (2019).

- Evidence for phospholipid export from the bacterial inner membrane by the Mia ABC transport system. *Nat. Microbiol.* **4**, 1692–1705.
- Jan, A.T. (2017). Outer membrane vesicles (OMVs) of gram-negative bacteria: a perspective update. *Front. Microbiol.* **8**, 1053.
- Kamischke, C., Fan, J., Bergeron, J., Kulasekara, H.D., Dalebroux, Z.D., Burrell, A., Kollman, J.M., and Miller, S.I. (2019). The *Acinetobacter baumannii* Mia system and glycerophospholipid transport to the outer membrane. *eLife* **8**, e40171.
- Kang, D., Gho, Y.-S., Suh, M., and Kang, C. (2002). Highly sensitive and fast protein detection with Coomassie brilliant blue in sodium dodecyl sulfate-polyacrylamide gel electrophoresis. *Bull. Kor Chem. Soc.* **23**, 1511–1512.
- King, J.E., and Roberts, I.S. (2016). Bacterial Surfaces: Front Lines in Host-Pathogen Interaction. *Adv. Exp. Med. Biol.* **915**, 129–56.
- Klein, S., Lorenzo, C., Hoffmann, S., Walther, J.M., Storbeck, S., Piekarski, T., Tindall, B.J., Wray, V., Nimtz, M., and Moser, J. (2009). Adaptation of *Pseudomonas aeruginosa* to various conditions includes tRNA-dependent formation of alanyl-phosphatidylglycerol. *Mol. Microbiol.* **71**, 551–565.
- Kolter, R., Inuzuka, M., and Helinski, D.R. (1978). Trans-complementation-dependent replication of a low molecular weight origin fragment from plasmid R6K. *Cell* **15**, 1199–1208.
- Kulkarni, H.M., Nagaraj, R., and Jagannadham, M.V. (2015). Protective role of *E. coli* outer membrane vesicles against antibiotics. *Microbiol. Res.* **181**, 1–7.
- Kulp, A., and Kuehn, M.J. (2010). Biological functions and biogenesis of secreted bacterial outer membrane vesicles. *Annu. Rev. Microbiol.* **64**, 163–184.
- Laemmli, U.K. (1970). Cleavage of structural proteins during the assembly of the head of bacteriophage T4. *Nature* **227**, 680–685.
- Lappann, M., Otto, A., Becher, D., and Vogel, U. (2013). Comparative proteome analysis of spontaneous outer membrane vesicles and purified outer membranes of *Neisseria meningitidis*. *J. Bacteriol.* **195**, 4425–4435.
- Leitner, D.R., Feichter, S., Schild-Prüfer, K., Rechberger, G.N., Reidl, J., and Schild, S. (2013). Lipopolysaccharide modifications of a cholera vaccine candidate based on outer membrane vesicles reduce endotoxicity and reveal the major protective antigen. *Infect. Immun.* **81**, 2379–2393.
- Lembke, M., Pennetzdorfer, N., Tutz, S., Koller, M., Vorkapic, D., Zhu, J., Schild, S., and Reidl, J. (2018). Proteolysis of ToxR is controlled by cysteine-thiol redox state and bile salts in *Vibrio cholerae*. *Mol. Microbiol.* **110**, 796–810.
- Li, C.C., Crawford, J.A., DiRita, V.J., and Kaper, J.B. (2000). Molecular cloning and transcriptional regulation of *ompT*, a ToxR-repressed gene in *Vibrio cholerae*. *Mol. Microbiol.* **35**, 189–203.
- Lichtenegger, S., Bina, I., Roier, S., Bauernfeind, S., Keidel, K., Schild, S., Anthony, M., and Reidl, J. (2014). Characterization of lactate utilization and its implication on the physiology of *Haemophilus influenzae*. *Int. J. Med. Microbiol.* **304**, 490–498.
- Lin, J., Huang, S., and Zhang, Q. (2002). Outer membrane proteins: key players for bacterial adaptation in host niches. *Microbes Infect.* **4**, 325–331.
- Lin, J., Zhang, W., Cheng, J., Yang, X., Zhu, K., Wang, Y., Wei, G., Qian, P.Y., Luo, Z.Q., and Shen, X. (2017). A *Pseudomonas* T6SS effector recruits PQS-containing outer membrane vesicles for iron acquisition. *Nat. Commun.* **8**, 14888.
- Malinverni, J.C., and Silhavy, T.J. (2009). An ABC transport system that maintains lipid asymmetry in the gram-negative outer membrane. *Proc. Natl. Acad. Sci. USA* **106**, 8009–8014.
- Manning, A.J., and Kuehn, M.J. (2011). Contribution of bacterial outer membrane vesicles to innate bacterial defense. *BMC Microbiol.* **11**, 258.
- Manoil, C. (1991). Analysis of membrane protein topology using alkaline phosphatase and beta-galactosidase gene fusions. *Methods Cell Biol.* **34**, 61–75.
- Matson, J.S., Livny, J., and DiRita, V.J. (2017). A putative *Vibrio cholerae* two-component system controls a conserved periplasmic protein in response to the antimicrobial peptide polymyxin B. *PLoS One* **12**, e0186199.
- Mey, A.R., Craig, S.A., and Payne, S.M. (2012). Effects of amino acid supplementation on porin expression and ToxR levels in *Vibrio cholerae*. *Infect. Immun.* **80**, 518–528.
- Miller, J.H. (1972). Experiments in molecular genetics (Cold Spring Harbor Laboratory).
- Miller, V.L., DiRita, V.J., and Mekalanos, J.J. (1989). Identification of *toxS*, a regulatory gene whose product enhances *toxR*-mediated activation of the cholera toxin promoter. *J. Bacteriol.* **171**, 1288–1293.
- Miller, V.L., and Mekalanos, J.J. (1988). A novel suicide vector and its use in construction of insertion mutations: osmoregulation of outer membrane proteins and virulence determinants in *Vibrio cholerae* requires *toxR*. *J. Bacteriol.* **170**, 2575–2583.
- Moisi, M., Jenul, C., Butler, S.M., New, A., Tutz, S., Reidl, J., Klose, K.E., Camilli, A., and Schild, S. (2009). A novel regulatory protein involved in motility of *Vibrio cholerae*. *J. Bacteriol.* **191**, 7027–7038.
- Moisi, M., Lichtenegger, S., Tutz, S., Seper, A., Schild, S., and Reidl, J. (2013). Characterizing the hexose-6-phosphate transport system of *Vibrio cholerae*, a utilization system for carbon and phosphate sources. *J. Bacteriol.* **195**, 1800–1808.
- Morales, V.M., Bäckman, A., and Bagdasarian, M. (1991). A series of wide-host-range low-copy-number vectors that allow direct screening for recombinants. *Gene* **97**, 39–47.
- O'Connor, A., and McClean, S. (2017). The role of universal stress proteins in bacterial infections. *Curr. Med. Chem.* **24**, 3970–3979.
- Osorio, C.G., Crawford, J.A., Michalski, J., Martinez-Wilson, H., Kaper, J.B., and Camilli, A. (2005). Second-generation recombination-based in vivo expression technology for large-scale screening for *Vibrio cholerae* genes induced during infection of the mouse small intestine. *Infect. Immun.* **73**, 972–980.
- Osorio, C.G., Martinez-Wilson, H., and Camilli, A. (2004). The *ompU* paralogue *vca1008* is required for virulence of *Vibrio cholerae*. *J. Bacteriol.* **186**, 5167–5171.
- Phillips, Z.N., Husna, A.U., Jennings, M.P., Seib, K.L., and Atack, J.M. (2019). Phasevarions of bacterial pathogens - phase-variable epigenetic regulators evolving from restriction-modification systems. *Microbiology* **165**, 917–928.
- Pressler, K., Vorkapic, D., Lichtenegger, S., Malli, G., Barilich, B.P., Cakar, F., Zingl, F.G., Reidl, J., and Schild, S. (2016). AAA+ proteases and their role in distinct stages along the *Vibrio cholerae* lifecycle. *Int. J. Med. Microbiol.* **306**, 452–462.
- Provenzano, D., and Klose, K.E. (2000). Altered expression of the ToxR-regulated porins *OmpU* and *OmpT* diminishes *Vibrio cholerae* bile resistance, virulence factor expression, and intestinal colonization. *Proc. Natl. Acad. Sci. USA* **97**, 10220–10224.
- Roier, S., Fenninger, J.C., Leitner, D.R., Rechberger, G.N., Reidl, J., and Schild, S. (2013). Immunogenicity of *Pasteurella multocida* and *Mannheimia haemolytica* outer membrane vesicles. *Int. J. Med. Microbiol.* **303**, 247–256.
- Roier, S., Zingl, F.G., Cakar, F., Durakovic, S., Kohl, P., Eichmann, T.O., Klug, L., Gadermaier, B., Weinzerl, K., Prassl, R., et al. (2016). A novel mechanism for the biogenesis of outer membrane vesicles in gram-negative bacteria. *Nat. Commun.* **7**, 10515.
- Salem, W., Leitner, D.R., Zingl, F.G., Schratte, G., Prassl, R., Goessler, W., Reidl, J., and Schild, S. (2015). Antibacterial activity of silver and zinc nanoparticles against *Vibrio cholerae* and enterotoxic *Escherichia coli*. *Int. J. Med. Microbiol.* **305**, 85–95.
- Schild, S., Nelson, E.J., Bishop, A.L., and Camilli, A. (2009). Characterization of *Vibrio cholerae* outer membrane vesicles as a candidate vaccine for cholera. *Infect. Immun.* **77**, 472–484.
- Schild, S., Nelson, E.J., and Camilli, A. (2008). Immunization with *Vibrio cholerae* outer membrane vesicles induces protective immunity in mice. *Infect. Immun.* **76**, 4554–4563.
- Schild, S., Tamayo, R., Nelson, E.J., Qadri, F., Calderwood, S.B., and Camilli, A. (2007). Genes induced late in infection increase fitness of *Vibrio cholerae* after release into the environment. *Cell Host Microbe* **2**, 264–277.
- Schwechheimer, C., and Kuehn, M.J. (2015). Outer-membrane vesicles from gram-negative bacteria: biogenesis and functions. *Nat. Rev. Microbiol.* **13**, 605–619.

- Seper, A., Fengler, V.H., Roier, S., Wolinski, H., Kohlwein, S.D., Bishop, A.L., Camilli, A., Reidl, J., and Schild, S. (2011). Extracellular nucleases and extracellular DNA play important roles in *Vibrio cholerae* biofilm formation. *Mol. Microbiol.* **82**, 1015–1037.
- Seper, A., Hosseinzadeh, A., Gorkiewicz, G., Lichtenegger, S., Roier, S., Leitner, D.R., Röhm, M., Grutsch, A., Reidl, J., Urban, C.F., and Schild, S. (2013). *Vibrio cholerae* evades neutrophil extracellular traps by the activity of two extracellular nucleases. *PLoS Pathog.* **9**, e1003614.
- Simonet, V.C., Baslé, A., Klose, K.E., and Delcour, A.H. (2003). The *Vibrio cholerae* porins OmpU and OmpT have distinct channel properties. *J. Biol. Chem.* **278**, 17539–17545.
- Tamayo, R., Schild, S., Pratt, J.T., and Camilli, A. (2008). Role of cyclic Di-GMP during el tor biotype *Vibrio cholerae* infection: characterization of the in vivo-induced cyclic Di-GMP phosphodiesterase CdpA. *Infect. Immun.* **76**, 1617–1627.
- Toyofuku, M., Nomura, N., and Eberl, L. (2019). Types and origins of bacterial membrane vesicles. *Nat. Rev. Microbiol.* **17**, 13–24.
- Urashima, A., Sanou, A., Yen, H., and Tobe, T. (2017). Enterohaemorrhagic *Escherichia coli* produces outer membrane vesicles as an active defence system against antimicrobial peptide LL-37. *Cell. Microbiol.* **19**, e12758.
- Warburg, O., and Christian, W. (1941). Isolierung und kristallisation des gärungsferments enolase. *Naturwissenschaften* **29**, 589–590.

STAR★METHODS

KEY RESOURCES TABLE

REAGENT or RESOURCE	SOURCE	IDENTIFIER
Antibodies		
Anti-mouse IgG, HRP-linked Antibody	Jackson ImmunoResearch	Cat#JIM-115-035-003; RRID: AB_10015289
A-OmpU Mouse serum	(Leitner et al., 2013)	N/A
A-OmpT Mouse serum	(Salem et al., 2015)	N/A
A-RpoA Mouse serum	BioLegend	Cat#663104; RRID: AB_2687386
Bacterial and Virus Strains		
DH5 α λ pir	(Kolter et al., 1978) (F ⁻ <i>endA1 glnV44 thi-1 recA1 relA1 gyrA96 deoR nupG</i> Φ 80d <i>lacZ</i> Δ M15 Δ (<i>lacZYA-argF</i>) U169 <i>hsdR17</i> (r _K ⁻ m _K ⁺) λ pirRK6)	N/A
SM10 λ pir	(Kolter et al., 1978) (<i>thi thr leu tonA lacY supE recA::RPA-2-Te::Mu</i> λ pir, Km ^R)	N/A
WT	(Miller et al., 1989) (AC53, wild type <i>V. cholerae</i> strain serogroup, O1; biotype, El Tor; serotype, Ogawa; spontaneous Sm ^R mutant of E7946; clinical isolate from Bahrain 1978; <i>hapR</i> ⁺ , Sm ^R)	N/A
WT ^{<i>lacZ</i>-}	(Tamayo et al., 2008) (insertion of <i>res</i> -cassette (<i>res-neo-sacB-res</i> cassette) in WT, Sm ^R , Km ^R)	N/A
Δ <i>yrbE</i>	(Roier et al., 2016) (Deletion of VC2519 in WT, Sm ^R)	N/A
Δ <i>yrbE</i> ^{<i>lacZ</i>-}	This paper (insertion of <i>res</i> -cassette (<i>res-neo-sacB-res</i> cassette) in Δ <i>yrbE</i> , Sm ^R , Km ^R)	N/A
Δ <i>almG</i>	This paper (Deletion of VC1577 in WT, Sm ^R)	N/A
Δ <i>yrbE</i> Δ <i>almG</i>	This paper (Deletion of VC2519 in Δ <i>almG</i> , Sm ^R)	N/A
<i>lacZ::araC</i>	This paper (Insertion of <i>araC</i> from pBADin <i>lacZ</i> in WT, Sm ^R)	N/A
<i>yrbE</i> [*]	This paper (Δ <i>yrbE</i> with reconstituted <i>yrbE</i> [*] allele harboring three silent point mutations located around stop codon of <i>yrbE</i> , exchanging AACTGATCA to AATTAACA Sm ^R)	N/A
<i>almG::phoA</i>	This paper (Insertion of pGP <i>phoA</i> in <i>almG</i> of WT, Sm ^R , Ap ^R)	N/A
Δ <i>yrbE</i> <i>almG::phoA</i>	This paper (Insertion of pGP <i>phoA</i> in <i>almG</i> of Δ <i>yrbE</i> , Sm ^R , Ap ^R)	N/A
<i>ompU::phoA</i>	This paper (Insertion of pGP <i>phoA</i> in <i>ompU</i> of WT, Sm ^R , Ap ^R)	N/A
Δ <i>yrbE</i> <i>ompU::phoA</i>	This paper (Insertion of pGP <i>phoA</i> in <i>ompU</i> of Δ <i>yrbE</i> , Sm ^R , Ap ^R)	N/A
<i>ompT::phoA</i>	This paper (Insertion of pGP <i>phoA</i> in <i>ompT</i> of WT, Sm ^R , Ap ^R)	N/A
Δ <i>yrbE</i> <i>ompT::phoA</i>	This paper (Insertion of pGP <i>phoA</i> in <i>ompT</i> of Δ <i>yrbE</i> , Sm ^R , Ap ^R)	N/A
Vc_res1_TRIVET <i>yrbF::tpc</i>	This paper (insertion of P _{tetA} controlled <i>tnpR</i> in Vc_res1 <i>yrbF::tpc</i> , Sm ^R , Cm ^R , Km ^R)	N/A

(Continued on next page)

Continued

REAGENT or RESOURCE	SOURCE	IDENTIFIER
Vc_res1 <i>yrbF::tpc</i>	This paper (insertion of <i>res</i> -cassette in <i>lacZ</i> in <i>yrbF::tpc</i> , Sm ^R , Cm ^R , Km ^R)	N/A
<i>yrbF::tpc</i>	This paper (insertion of <i>tetRphoAcat</i> downstream of <i>yrbF</i> in WT, Sm ^R , Cm ^R)	N/A
Chemicals, Peptides, and Recombinant Proteins		
Polymyxin B sulfate salt	Sigma-Aldrich	Cat#P4932
Bile salts	Sigma-Aldrich	Cat#B8756
Sodium dodecylsulfate (SDS)	Bio-Rad	Cat#161-0302
TRIzol Reagent	ThermoFisher	Cat#15596026
Critical Commercial Assays		
IscripT cDNA synthesis Kit	Biorad	Cat#1708890
RNAse free DNaseI Kit	Promega	Cat#9PIM610
RNA isolation Kit Rneasy	Quiagen	Cat#74106
Monarch Total RNA Miniprep Kit	New England Biolabs	Cat#T2010S
PeqGOLD total RNA Kit	VWR	Cat#732-2868
SYBR GreenER™ qPCR SuperMix for ABI PRISM™ Instrument	ThermoFisher	Cat#11760
Experimental Models: Organisms/Strains		
CD-1® IGS Mouse	Charles River	Cat#Crl:CD1(ICR); RRID: IMSR_CRL:022
Oligonucleotides		
For more oligonucleotides, see Table S1	N/A	N/A
qPCR_yrbE_1 GTTCGCCAGTTATACAGCATTG	(Roier et al., 2016)	N/A
qPCR_yrbE_2 CTGAGCACCATGCCAATAAAG	(Roier et al., 2016)	N/A
qPCR_vacJ_1 AGTTTCGCAAGAGGCCTTATTA	(Roier et al., 2016)	N/A
qPCR_vac_2 AGCTTGCCGTTGGAGATAAG	(Roier et al., 2016)	N/A
qPCR-VCr001_1 AGGGAGGAAGGTGGTTAAGT	(Fengler et al., 2012)	N/A
qPCR-VCr001_2 CGCTACACCTGAAATTCTACCC	(Fengler et al., 2012)	N/A
yrbE*_test GCATTGATGTTTGGGAATTAAG	This paper	N/A
yrbE*_seq AAACCCGGGCTCCGCCACATC TTCACGTT	This paper	N/A
qPCR-VCr001_2 CGCTACACCTGAAATTCTACCC	(Fengler et al., 2012)	N/A
Recombinant DNA		
Plasmid pBAD18	(Guzman et al., 1995)	N/A
Plasmid pCVD442	(Donnenberg and Kaper, 1991)	N/A
Plasmid pCVDyrbF::tpc	This paper (pCVD442 with <i>irgA::tetRphoAcat</i> , Ap ^R , Cm ^R)	N/A
Plasmid pCVDyrbE*	This paper (pCVD442 with point mutated <i>yrbE</i> fragment, Ap ^R)	N/A

(Continued on next page)

Continued

REAGENT or RESOURCE	SOURCE	IDENTIFIER
Plasmid pCVDΔalmG	This paper (pCVD442 with up- and downstream fragments of <i>almG</i> , Ap ^R)	N/A
Plasmid pCVDlacZ::araC	This paper (pCVD442 with <i>araC</i> flanked by up- and downstream fragments of <i>lacZ</i> , Ap ^R)	N/A
Plasmid pCVDyrbF-B ^{PARA}	This paper (pCVD442 with the arabinose-inducible promoter flanked by up- and downstream fragments of the <i>yrb</i> promoter, Ap ^R)	N/A
Plasmid pGPphoA	(Moisi et al., 2009)	N/A
Plasmid pGPphoAalmG	This paper (pGPphoA with 'almG' fragment to generate transcriptional <i>phoA</i> -fusions to the <i>almGEF almEFG</i> promoter, Ap ^R)	N/A
Plasmid pGPphoAompU	(Lembke et al., 2018) (pGPphoA with 'ompU' fragment to generate transcriptional <i>phoA</i> -fusions to the <i>ompU</i> promoter, Ap ^R)	N/A
Plasmid pGPphoAompT	(Lembke et al., 2018) (pGPphoA with 'ompT' fragment to generate transcriptional <i>phoA</i> -fusions to the <i>ompT</i> promoter, Ap ^R)	N/A
Plasmid p	(Morales et al., 1991) (pMMB67EH, IncQ broad-host-range low-copy-number cloning vector, IPTG-inducible, Apr)	N/A
Plasmid pRes1	(Osorio et al., 2005) (pSL111 with <i>res1-neo-sacB-res1</i> cassette, Km ^R)	N/A
Plasmid pyrBF-B	This paper (expression plasmid with <i>yrb</i> operon (VC2516-VC2520) in pMMB67EH, Ap ^r)	N/A
Software and Algorithms		
Prism 5.0	GraphPad	https://www.graphpad.com
ImageLab Software	BioRad	https://www.bio-rad.com
Corel Draw	Corel Corporation	https://www.coreldraw.com

LEAD CONTACT AND MATERIALS AVAILABILITY

Further information and requests for resources and reagents should be directed to and will be fulfilled by the Lead Contact, Stefan Schild (stefan.schild@uni-graz.at). All reagents generated in this study are available from the Lead Contact with a completed Materials Transfers Agreement.

EXPERIMENTAL MODEL AND SUBJECT DETAILS

Housing Conditions for Experimental Animals

5 to 6 day old CD-1 mice (CrI:CD1, Charles River Laboratories) of both genders were used in all experiments in accordance with the rules of the ethics committee at the University of Graz and the corresponding animal protocol, which has been approved by the Austrian Federal Ministry of Science and Research Ref. II/10b. Mice were housed with food and water ad libitum and monitored under the care of full-time staff.

Competition Assay

Competition assays in infant mice (*in vivo* assay), LB broth or minimal media M9 were performed with WT, deletion mutants, or WT pyrBF-B (*lacZ*⁺) competed for ~22 h against isogenic WT, deletion mutants, or WT strain carrying an empty vector (*lacZ*⁻) essentially as previously described (Camilli and Mekalanos, 1995; Schild et al., 2007). The individual strains and conditions used for each competition are indicated along the presentation of the respective data set. Briefly, strains were grown on LB plates or in minimal media M9 (M9, M9^{ToxR1} or M9^{ToxR1/Alm1}) overnight (O/N), diluted to OD₆₀₀ = 0.002 in a 1:1 ratio, and used to intragastrically inoculate

infant mice (5-day-old CD-1 mice). Appropriate dilutions of the inoculum were plated on LB-Sm/X-Gal or on LB-Ap/X-Gal plates in case of *V. cholerae* strains harboring a plasmid to determine the exact input ratio. Approximately 22 h post-infection mice were euthanized, their small bowels were removed and homogenized in 1 ml of LB with 15% glycerol. *In vitro* competitions in LB or minimal media M9 were performed in parallel by inoculation of 2 ml liquid culture with $\sim 10^5$ CFU from the inoculum and subsequent incubation for ~ 22 h at 37°C with aeration. CFU were determined by plating appropriate dilutions of the homogenized intestine or culture grown *in vitro* on LB-Sm/X-Gal or on LB-Ap/X-Gal plates in case of *V. cholerae* strains harboring a plasmid. Results are given by the competition index (CI), which is the ratio of *lacZ*⁺-CFU to *lacZ*⁻-CFU normalized for the input ratio. If applicable, plasmid maintenance was determined along the competitions *in vivo* and *in vitro* by calculating dividing the respective Ap^R-CFU (LB-Ap/X-Gal plates) by the Sm^R-CFU (LB-Sm/X-Gal).

Resolution Assay

Resolution assay was performed as previously described (Cakar et al., 2018). To quantify resolution, strain Vc_res1_TRIVET *yrbF::tpc* was grown O/N on LB-Sm/Km/Ap plates and adjusted in LB-Sm/Km/Ap to OD₆₀₀=1, which was used as inoculum. To determine *in vitro* resolution frequencies, the inoculum was diluted 1:100 in 5 ml of LB-Sm/Ap, LB-Sm/Ap supplemented with 75 μM of 2,2'-bipyridyl or 100 μM of FeSO₄ and incubated for 8 h. To determine the *in vivo* resolution, the inoculum was diluted 1:500 in LB and anesthetized 5-day old CD-1 mice were intragastrically inoculated with 50 μl of this dilution ($\sim 10^6$ CFU per mouse). Mice were euthanized at 6 or 22 h post-infection time, and bacteria were recovered from intestine. At the given time point, the amount of resolution *in vitro* and *in vivo* was determined by plating appropriate dilutions on LB-Sm/Km and LB-Sm/Ap plates. Results were expressed as % resolution, calculated as the Sm^R/Km^S CFU (Sm^R/Ap^R CFU minus Sm^R/Km^R CFU) divided by Sm^R/Ap^R CFU.

Infection Studies to Obtain Bacterial RNA

For *in vivo* studies, anesthetized 5-day old CD-1 mice were intragastrically inoculated with 50 μL of WT adjusted to OD₆₀₀ of 0.002 in LB, corresponding to an infection dose of $\sim 10^6$ CFU per mouse. After 22h, mice were euthanized, and small intestine was removed and mechanically homogenized in 1.5 mL of TRIzol Reagent (Thermo Fisher Scientific).

METHOD DETAILS

Bacterial Strains and Growth Conditions

Bacterial strains, plasmids and oligonucleotides used in this study are listed in the “Key Resources Table”. The clinical isolate *V. cholerae* O1 El Tor E7946 (Miller et al., 1989) served as wild type (WT) strain in all experiments. Unless stated otherwise, all *V. cholerae* strains were grown with aeration in Lura Bertani (LB) broth or minimal medium M9 according to standard recipe (Miller, 1972) at 37°C. *E. coli* strains DH5αλpir and SM10λpir (Miller and Mekalanos, 1988) were used for genetic manipulations and grown with aeration in LB broth at 37°C. Unless stated otherwise, minimal media M9 compositions are abbreviated as follows: M9 for minimal media M9 supplemented with glucose; M9^{ToxR1} for minimal media M9 supplemented with glucose, asparagine, arginine, glutamate and serine; M9^{ToxR1/Alm1} for minimal media M9 supplemented with glucose, asparagine, arginine, glutamate, serine and sub-MIC concentrations of polymyxin B (PMB, 3 μg/ml or 0.3 μg/ml for strains with $\Delta almG$ background, respectively). Antibiotics and other supplements were used in the following final concentrations: streptomycin (Sm, 100 μg ml⁻¹), ampicillin (Ap, 50 μg ml⁻¹ in combination with other antibiotics, otherwise 100 μg ml⁻¹), sucrose (10%), glucose (0.2%), arabinose (Ara, 0.2%), asparagine (25 mM) arginine (25 mM), glutamate (25 mM), and serine (25 mM).

Genetic Manipulations

The isolation of chromosomal DNA, PCR reactions, the purification of plasmids or PCR products, the construction of suicide and expression plasmids as well as the subsequent generation of deletion mutants were carried out as described previously (Pressler et al., 2016; Seper et al., 2011). Qiagen plasmid kits were used for isolation of plasmid DNA, Qiaquick® Gel extraction and Qiaquick® PCR Purification kits (Qiagen) were used for purifying DNA fragments. PCR reactions for subcloning were carried out using the Q5® High-Fidelity DNA Polymerase (NEB), while Taq DNA Polymerase (NEB) was used for all other PCRs. Constructions of in-frame *almG* deletion mutants were carried out as described by Donnenberg and Kaper (Donnenberg and Kaper, 1991). Briefly, ~ 800 bp PCR fragments located up- and downstream of the gene of interest were amplified using the oligonucleotide pairs *almG*_XbaI_1 and *almG*_BamHI_2 as well as *almG*_BamHI_3 and *almG*_SacI_4. After digestion of the PCR fragments with the appropriate restriction enzyme (NEB) indicated by the name of the oligonucleotide, they were ligated into pCVD442, which was digested with the appropriate restriction enzymes.

Complementation of *yrbE* was achieved either *in trans* by using the expression plasmid *pyrBE* (Roier et al., 2016) or by re-insertion of a slightly modified *yrbE*^{*} allele (altered nucleotide sequence in the wobble position of some codons, resulting in identical amino acid sequence compared to the WT allele) in the original chromosomal gene locus to avoid the usage of antibiotics for plasmid maintenance. The latter was constructed via PCR fragments amplified using the oligonucleotide pairs VC2519_XbaI_up_fw and comp_*yrbE*^{*}_1 as well as comp_*yrbE*^{*}_2 and VC2519_XmaI_down_rv and subsequent splicing by overlap extension (SOE) PCR of the two purified PCR fragments introducing three silent point mutations changing AACTGATCA to AATTAACA located around stop codon of *yrbE*. The SOE PCR fragment was digested with XmaI and XbaI (NEB), ligated into a similar digested pCVD442 resulting in pCVD^{yrbE}^{*}.

In case of the suicide vector pCVDlacZ::araC used for *araC* insertion into the *lacZ*-locus of *V. cholerae* ~800 bp PCR fragments flanking *lacZ* were amplified using the oligonucleotide pairs lacZ_XbaI_1 and lacZ_BamHI_2 as well as lacZ_SphI_3 and lacZ_SacI_4, while *araC* was amplified from pBAD18 using the oligonucleotide pairs araC_BamHI_1 and araC_EcoRI_2. All fragments were digested using the restriction enzymes, indicated by the name of oligonucleotide To construct the suicide vector pCVDyrbF-B^{pARA}, replacing the natural *yrb*-promoter with an arabinose-inducible promoter, ~800 bp PCR fragments flanking the *yrb*-promoter were amplified using the oligonucleotide pairs yrb_SacI_1 and yrb_SphI_2 as well as yrb_EcoRI_3 and yrb_XbaI_4, while the fragment harboring the arabinose-inducible promoter was amplified from pBAD18 using the oligonucleotide pairs pARA_SphI_1 and pARA_EcoRI_2. After digestion with the restriction enzymes, indicated by the name of oligonucleotide, PCR fragments were ligated into pCVD442, restricted with appropriate restriction enzymes (NEB).

The suicide vectors pGPphoA-almG, pGPphoA-ompU and pGPphoA-ompT for chromosomal insertion were constructed to obtain chromosomal transcriptional fusions of promoterless *phoA* to *almG* (*almG*::*phoA*), *ompU* (*ompU*::*phoA*) and *ompT* (*ompT*::*phoA*), as PhoA acts as a reporter for gene expression in *V. cholerae*. DNA fragments containing the upstream region of *almG*, *ompU* and *ompT* were amplified by PCR using oligonucleotide pair almG_pGPphoA_XbaI and almG_pGPphoA_KpnI, the PCR product was digested with the restriction enzymes indicated and ligated with similarly digested pGPphoA.

For construction of the expression plasmid pyrbF-B the entire *yrb*-operon was amplified with oligonucleotides yrb_operon_SacI_1, yrb_operon_XbaI_2, the PCR fragment was digested with the appropriate restriction enzymes and ligated into a similar digested pMMB67EH.

Unless noted otherwise, ligation products were transformed into DH5 α *pir* and Ap^R colonies were characterized for the correct constructs by PCR (and restriction analysis).

To obtain insertion and deletion strains generated derivatives of the pGPphoA or pCVD442 were transformed into *E. coli* Sm10 λ *pir* and conjugated into *V. cholerae*. Exconjugants were purified by Sm^R/Ap^R selection. In the case of pCVD442 derivatives sucrose selection was used to obtain Ap^S colonies and chromosomal deletions/replacements were confirmed by PCR, respectively. To generate the complementation strain *yrbE** the pCVDyrbE* was mobilized into Δ *yrbE*, exconjugants were purified by Sm^R/Ap^R selection and finally sucrose selection was used to obtain Ap^S colonies. Correct chromosomal insertion of the *yrbE** allele was confirmed via PCR using a discriminator oligonucleotide pair yrbE*_test and VC2519_XmaI_down_rv as well as via sequencing using yrbE*_seq.

Resolution Assay

Resolution assay was performed as previously described (Cakar et al., 2018). To quantify resolution, strain Vc_res1_TRIVET *yrbF*::*tpc* was grown O/N on LB-Sm/Km/Ap plates and adjusted in LB-Sm/Km/Ap to OD₆₀₀=1, which was used as inoculum. To determine *in vitro* resolution frequencies, the inoculum was diluted 1:100 in 5 ml of LB-Sm/Ap, LB-Sm/Ap supplemented with 75 μ M of 2,2'-bipyridyl or 100 μ M of FeSO₄ and incubated for 8 h. To determine the *in vivo* resolution, the inoculum was diluted 1:500 in LB and anesthetized 5-day old CD-1 mice were intragastrically inoculated with 50 μ l of this dilution (~10⁶ CFU per mouse). Mice were euthanized at 6 or 22 h post-infection time, and bacteria were recovered from intestine. At the given time point, the amount of resolution *in vitro* and *in vivo* was determined by plating appropriate dilutions on LB-Sm/Km and LB-Sm/Ap plates. Results were expressed as % resolution, calculated as the Sm^R/Km^S CFU [Sm^R/Ap^R CFU minus Sm^R/Km^R CFU] divided by Sm^R/Ap^R CFU.

Quantitative Real-time PCR

Expression of *yrbE* and *vacJ* was determined by quantitative real-time RT-PCR (qRT-PCR). For *in vitro* studies, WT was grown to an OD₆₀₀ of 0.5 to 0.8 in LB, while the arabinose-inducible *yrbF*-B variant was grown to an OD₆₀₀ of approximately 0.8 in M9^{ToxR1} with (w) or without (w/o) arabinose (Ara). Bacterial RNA extraction, DNase digestion, cDNA synthesis, and qRT-PCR were performed as described previously (Lichtenegger et al., 2014). For *in vivo* studies, anesthetized 5-d-old CD-1 mice were intragastrically inoculated with 50 μ l of WT adjusted to OD₆₀₀ of 0.002 in LB, corresponding to an infection dose of ~10⁶ CFU per mouse. After 22 h, mice were euthanized, and small intestine was removed and mechanically homogenized in 1.5 mL of TRIzol Reagent (Thermo Fisher Scientific). RNA was isolated using either the Monarch Total RNA Miniprep Kit (New England Biolabs) or the RNA isolation Kit Rneasy (Quiagen) for *in vitro* samples grown in LB as well as *in vivo* samples or the PeqGOLD total RNA Kit (Peqlab) for *in vitro* samples grown in minimal media M9 according to the manufacturer's protocols, and chromosomal DNA was digested by using RQ1 RNase-Free DNase (Promega). Synthesis of cDNA and qRT-PCR were performed as described previously using the iScript Select cDNA Synthesis Kit (Bio-Rad) and the SYBR GreenER qPCR SuperMix for ABI PRISM [(Thermo Fisher Scientific); (Seper et al., 2013)]. Each cDNA sample was tested in triplicate. The sequences of the primers used for qRT-PCR starting with "qPCR_" are listed in the "Key Resources Table". Results were analyzed using StepOne Software v2.1, and relative gene expression comparisons were calculated by the mean cycle threshold of samples, which were normalized to the housekeeping gene 16S rRNA (VCr001) and to one randomly selected *in vitro* reference sample.

Isolation of Lipid A

The protocol for large scale lipid A extraction as described by Henderson and coworkers was used (Henderson et al., 2013). Briefly 500 ml of respective culture were harvested, washed with PBS and resuspended in 40 ml PBS. Subsequently 50 ml of chloroform and 100 ml of methanol were added to create a single-phase Bligh-Dyer mixture. Samples were washed with

single-phase Bligh-Dyer mixture and resuspended in 54 ml of mild acid hydrolysis buffer. Samples were boiled for 1 h and then converted to a two-phase Bligh-Dyer mixture by adding 60 ml of chloroform and 60 ml of methanol. The lower phase was extracted and a second extraction was performed using the lower phase of a pre-equilibrated two-phase Bligh-Dyer mixture. Both lower phases were pooled and washed with new upper phase of a pre-equilibrated two-phase Bligh-Dyer mixture and dried for subsequent usage.

Analysis of Lipid A by LC-MS

Normal phase LC-MS was performed using an Agilent 1200 Quaternary LC system coupled to a high-resolution TripleTOF5600 mass spectrometer (Sciex, Framingham, MA). A Unison UK-Amino column (3 μm , 25 cm \times 2 mm) (Imtakt USA, Portland, OR) was used. Mobile phase A consisted of chloroform/methanol/aqueous ammonium hydroxide (800/195/5, v/v/v). Mobile phase B consisted of chloroform/methanol/water/aqueous ammonium hydroxide (600/340/50/5, v/v/v/v). Mobile phase C consisted of chloroform/methanol/water/aqueous ammonium hydroxide (450/450/95/5, v/v/v/v). The elution program consisted of the following: 100% mobile phase A was held isocratically for 2 min and then linearly increased to 100% mobile phase B over 14 min and held at 100% B for 11 min. The LC gradient was then changed to 100% mobile phase C over 3 min and held at 100% C for 3 min, and finally returned to 100% A over 0.5 min and held at 100% A for 5 min. The total LC flow rate was 300 $\mu\text{l}/\text{min}$. The MS settings are as follows: Ion spray voltage (IS) = -4500 V, Curtain gas (CUR) = 20 psi, Ion source gas 1 (GS1) = 20 psi, De-clustering potential (DP) = -55 V, and Focusing Potential (FP) = -150 V. Nitrogen was used as the collision gas for MS/MS experiments. Data acquisition and analysis were performed using Analyst TF1.5 software (Sciex, Framingham, MA). High-resolution mass spectra and isotope patterns allowed a precise identification of the respective lipid A species. It should be noted that preparation of lipid A extracts derived from *V. cholerae* requires high culture volume and is labor-intensive. Thus, lipid A samples were prepared in batches and subjected to LC-MS analysis within two weeks to minimize artefact formation and sample degradation. Variations in LC retention times for the respective lipid A species can occur between different batches analyzed in different runs due to changes in column and solvent conditions.

Preparation of OMVs

In general, OMV were isolated as described previously with minor adaptations (Schild et al., 2009). O/N cultures of the respective strains were cultivated in M9, diluted 1:100 in M9^{ToxR \uparrow} or M9^{ToxR \uparrow} with arabinose and grown for 4 or 8 h at 37°C and 180 rpm, before the cells were removed from the supernatant by centrifugation (9000 \times g, 15 min). The supernatant was filtered through 0.22 μm pore size filters to remove intact cells. OD₆₀₀ of each culture was determined by photometric measurements using a Beckman Coulter DU730 spectrophotometer for subsequent OMV quantification. To ensure that no bacteria were left in the supernatant, 1 ml of the filtrate was plated on LB-agar plates and incubated at 37°C O/N. The OMVs present in the supernatant were pelleted through subsequent ultracentrifugation (150,000 g, 4°C, 4 h) as previously described (Schild et al., 2009). Protein concentration was determined using Bradford assay (Bio-Rad Laboratories, Protein Assay Dye Reagent) according to the manufacturer's manual and normalized to the OD₆₀₀ of the respective culture.

Preparation of Outer Membrane Proteins and Whole Cell Lysates

Proteins of the outer membrane were essentially prepared as previously published (Carlone et al., 1986; Roier et al., 2013; Salem et al., 2015). O/N cultures of the respective strains were cultivated in M9 and diluted 1:100 in M9^{ToxR \uparrow} . At the indicated time point cultures of *V. cholerae* were harvested by centrifugation (3,200 g, 10 min, 4°C), washed once in HEPES buffer (10 mM, pH 7.4) and resuspended in 0.75 ml HEPES buffer (10 mM, pH 7.4). Then the suspension was transferred in a cryo-tube and cells were disrupted by homogenization with 0.1 mm glass beads in combination with a PowerLyzerTM 24 (MO BIO Laboratories, Inc.), applying three times, 1 min cycles at 3400 rpm with 1-min intervals on ice between each cycle. Unbroken cells were removed by centrifugation (13,000 g, 5 min, 4°C). The supernatant containing the outer membrane material was transferred into a new tube and centrifuged again (16,100 g, 30 min). The membrane pellet was re-suspended in 0.4 ml HEPES buffer (10 mM, pH 7.4). To solubilize the cytoplasmic membrane, 0.4 ml HEPES buffer (10 mM, pH 7.4) with 2% sarcosyl was added and incubated at room temperature and constant shaking for 30 min. After centrifugation (16,100 g, 30 min), the pellet containing proteins of the outer membrane was washed once with 0.5 ml HEPES buffer (10 mM, pH 7.4) and finally re-suspended in 50 μl HEPES buffer (10 mM, pH 7.4). Purified outer membrane preparations were stored at -20°C. The protein concentrations of outer membrane preparations were determined by photometric measurements of the absorbances at 260 nm and 280 nm using a Beckman Coulter DU730 spectrophotometer in combination with a TrayCell (Hellma) and the Warburg-Christian equation given as mg protein/ml = [(1.31 \times A280) - (0.57 \times A260)] \times dilution factor (Warburg and Christian, 1941).

For whole cell lysates, equal amounts of cells (equivalent to 1.3 ml of an OD₆₀₀=1) were harvested by centrifugation (3,200 \times g, 10 min, 4°C) from the respective *V. cholerae* cultures. Cell pellets were directly resuspended in 53 μl SDS-PAGE sample buffer (Laemmli, 1970), boiled for 10 min and subjected to SDS-PAGE.

SDS-PAGE and Immunoblot

Proteins were separated by sodium dodecyl sulfate-polyacrylamide gel electrophoresis (SDS-PAGE) using polyacrylamide (15%) gels in combination with the Mini-PROTEAN Tetra cell system (Bio-Rad, Vienna) (Laemmli, 1970). As molecular mass standard Pre-stained Protein Marker Broad Range (New England Biolab) or PageRulerTM Prestained Protein Ladder 10 to 180 kDa (Thermo Fisher)

were used as indicated. Subsequently protein bands were visualized according to Kang et al. (Kang et al., 2002) or further processed for immunoblot analysis as previously described (Schild et al., 2008). As primary antibodies (anti-OmpU, anti-OmpT and anti-RpoA) generated in mice were used [(Leitner et al., 2013; Salem et al., 2015) and BioLegend]. HRP-linked anti-mouse IgG was used as secondary antibody. Chemiluminescence detection was performed by using the Immuno-Star™ WesternC™ Kit (Bio-Rad Laboratories) and subsequent exposure in a ChemiDoc XRS system (Bio-Rad Laboratories) in combination with Quantity One software (Bio-Rad Laboratories).

Growth Kinetics

Growth kinetics were essentially performed as previously described in transparent 24-well plates (Greiner) with 1 ml culture volume (Gumpenberger et al., 2016; Moisi et al. 2013; Seper et al. 2011). Briefly, the respective strains were grown in a pre-culture for ~16 h in M9 with aeration and shaking at 37°C. For growth assays of the WT, $\Delta yrbE$ mutant or *yrbE** complementation strain, pre-cultures were adjusted to $OD_{600} = 0.05$ in M9 or $M9^{ToxR\uparrow/Alm\uparrow}$ [(di)glycine-modified lipid A activating conditions using sub-MIC PMB concentrations (3 $\mu\text{g/ml}$)] and allowed to adapt for 2 h before OD_{600} measurements started. For growth assays of the arabinose-inducible *yrbF-B* variant, pre-cultures with arabinose were pelleted by centrifugation (6000 x g, 10 min), resuspended in fresh M9 or $M9^{ToxR\uparrow}$, adjusted to $OD_{600} = 0.05$ in either M9 with or without arabinose or $M9^{ToxR\uparrow}$ with or without arabinose and allowed to adapt for 2 h in the new medium. In case of $M9^{ToxR\uparrow}$ with or without arabinose, bile was added to final concentration of 0.1% after the 2h adaptation phase. In all cases, the OD_{600} was monitored every 30 min in the SPECTROstar^{Nano} microplate reader (BMG Labtech) at 37°C with shaking. For presentation of data, mean of at least four independent growth curves were plotted and area under curve (AUC) values were calculated by GraphPad prism version 5.01.

Minimal Inhibitory Concentration (MIC)-assays

For MIC assays O/N cultures of *V. cholerae* WT, $\Delta yrbE$ mutant or *yrbE** complementation strain were either grown in M9 or $M9^{ToxR\uparrow/Alm\uparrow}$ [(di)glycine-modified lipid A activating conditions using sub-MIC PMB concentrations (3 $\mu\text{g/ml}$)] as well as $\Delta almG$ or $\Delta almG\Delta yrbE$ were grown in M9. O/N cultures were shifted into fresh M9 or $M9^{ToxR\uparrow/Alm\uparrow}$ [(di)glycine-modified lipid A activating conditions using sub-MIC PMB concentrations (3 $\mu\text{g/ml}$ or 0.3 $\mu\text{g/ml}$ for strains with $\Delta almG$ background, respectively)] to a final concentration of 10^6 CFU/ml. The arabinose-inducible *yrbF-B* variant was grown O/N in M9 with arabinose or $M9^{ToxR\uparrow}$ with arabinose. To remove residual arabinose, the O/N cultures were pelleted by centrifugation (6000 x g, 10 min), resuspended in fresh M9 and then diluted into M9 with or without arabinose to a final concentration of 10^6 CFU/ml. Alternatively, O/N cultures were pelleted by centrifugation (6000 x g, 10 min), resuspended in fresh $M9^{ToxR\uparrow}$ and diluted into $M9^{ToxR\uparrow}$ with or without arabinose to a final concentration of 10^6 CFU/ml.

In all cases, bacteria were allowed to adapt for ~2 h, before 100 μl of the bacterial culture were placed into 96-well plates and 10 μl of appropriate serial dilutions of the respective antimicrobial agent (bile salts, additional PMB, SDS) were added. Two-fold serial dilutions of antimicrobial agents were tested in the following final concentrations: 8% to 0.0078% for bile salts, 3,200 $\mu\text{g/ml}$ to 0.39 $\mu\text{g/ml}$ for PMB and 0.25% to 0.0078% for SDS. After 18h incubation in a humid chamber at 37°C OD_{600} was measured using the Spectrostar^{NANO} Microplate Reader (BMG Labtech). The MIC was defined as the lowest antimicrobial agent concentration, which inhibited bacterial growth. Growth was defined by an at least three-fold increase of the OD_{600} compared to the respective sterile control (M9 with or without arabinose or $M9^{ToxR\uparrow}$ with or without arabinose).

Survival Assays

V. cholerae WT, $\Delta yrbE$ mutant or the complementation strain *yrbE** were grown O/N in M9, adjusted to an $OD_{600} = 0.001$ in 25 ml $M9^{ToxR\uparrow}$ before PMB was added to a final concentration of 3 $\mu\text{g/ml}$. For survival assays in presence of bile, the arabinose-inducible *yrbF-B* variant was grown O/N in M9 with arabinose, washed once in $M9^{ToxR\uparrow}$ and then adjusted in 25 ml $M9^{ToxR\uparrow}$ with or without arabinose to an $OD_{600} = 0.001$. After an adaptation for 2 h in $M9^{ToxR\uparrow}$ (activating OmpU/T switch) bile salts (0.1 %) were added. In general, samples were taken just before addition of PMB or bile salts (0 h), as well as 2, 4, 8 and 24 h after addition of the antimicrobial agent and appropriate dilutions were plated on LB plates. Percent survival for 2, 4, 8 and 24 h was calculated by the determined CFU at the respective time point divided by the determined CFU at 0 h multiplied by 100.

Alkaline Phosphatase Assays

To determine the enzymatic activities for the transcriptional *ompU::phoA*, *ompT::phoA* and *almG::phoA* fusion, alkaline phosphatase assays were performed as described previously (Manoil, 1991). Briefly, bacterial cultures were shifted from M9 to $M9^{ToxR\uparrow}$ in case of *ompU::phoA* and *ompT::phoA* or shifted from M9 to $M9^{ToxR\uparrow/Alm\uparrow}$ in case of *almG::phoA*. Subsequently, bacterial cultures were harvested after 0, 1, 2, 4 and 8 h and subjected to the alkaline phosphatase assays. The activities were expressed in Miller units, given by $(A_{405} \times 1,000)/(A_{600} \times \text{ml} \times \text{min})$.

QUANTIFICATION AND STATISTICAL ANALYSIS

Data sets are presented as mean with standard deviation (SD) in case of normal distribution or as median with interquartile range (IQR) in case of non-gaussian distribution. Statistical analyses were performed using GraphPad Prism 5.0 as follows: unpaired t-test (single comparison) or one-way Anova followed by Bonferroni's post test (multiple comparisons) in case of normal distribution

(data sets presented as mean with SD) or Mann–Whitney U test (single comparison) or Kruskal–Wallis followed by Dunn’s post test (multiple comparisons) in case of non-gaussian distribution (data sets presented as median with IQR). A *P* value of less than 0.05 was considered significant and indicated by an asterisk ($*P < 0.05$). Unless stated otherwise, the number of biological replicates for each data set is given by “n” and is provided in the respective figure legend.

DATA AND CODE AVAILABILITY

This study did not generate/ analyze datasets/ codes.